Exploiting vulnerabilities induced by recurrent mutations in chondrosarcoma and giant cell tumour of bone: therapeutic targeting of the altered epigenome and beyond

Venneker, S.

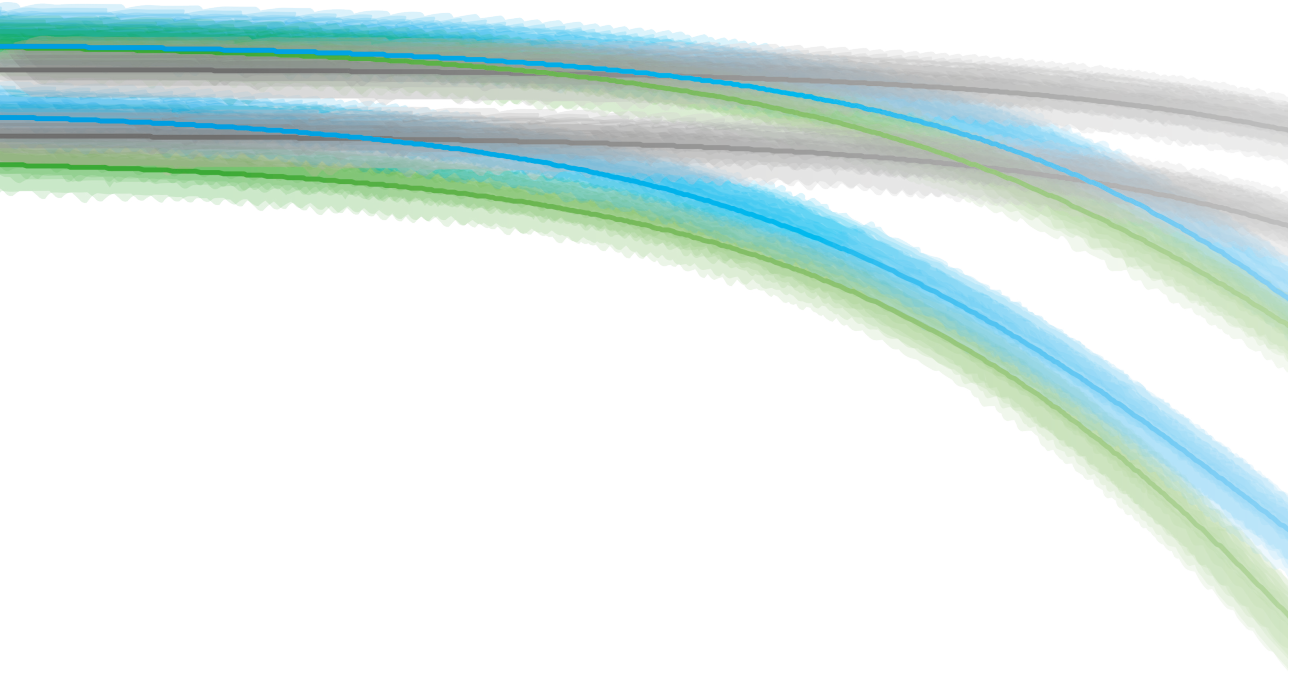

Chapter 4

Beyond the influence of *IDH* mutations: Exploring epigenetic vulnerabilities in chondrosarcoma

Sanne Venneker, Alwine B. Kruisselbrink, Zuzanna Baranski, Ieva Palubeckaitė, Inge H. Briaire-de Bruijn, Jan Oosting, Pim J. French, Erik H.J. Danen, and Judith V.M.G. Bovée

Cancers 2020; 12(12):3589

Simple summary

Cartilage tumors frequently harbor mutations in the isocitrate dehydrogenase *(IDH1* or *IDH2*) genes. These mutations cause an increase in the levels of the oncometabolite D-2-hydroxyglutarate (D-2-HG), which leads to widespread changes in several cellular processes, including the epigenetic landscape. The aim of our study was to explore whether the methylome of *IDH* mutant cartilage tumors is altered upon tumor progression and whether these underlying epigenetic vulnerabilities could be used as a target for therapy in both *IDH* wildtype and *IDH* mutant high-grade chondrosarcomas. As surgery is nowadays the only treatment option for chondrosarcoma patients, the identification of novel therapeutic strategies remains an important endeavor. The findings in this study show that histone deacetylase (HDAC) inhibition may represent a promising therapeutic strategy for all chondrosarcoma patients, since sensitivity towards this therapeutic option seems independent of the *IDH* mutation status and the chondrosarcoma subtype.

Abstract

Mutations in the isocitrate dehydrogenase (*IDH1* or *IDH2*) genes are common in enchondromas and chondrosarcomas, and lead to elevated levels of the oncometabolite D-2-hydroxyglutarate causing widespread changes in the epigenetic landscape of these tumors. With the use of a DNA methylation array, we explored whether the methylome is altered upon progression from *IDH* mutant enchondroma towards high-grade chondrosarcoma. High-grade tumors show an overall increase in the number of highly methylated genes, indicating that remodeling of the methylome is associated with tumor progression. Therefore, an epigenetics compound screen was performed in five chondrosarcoma cell lines to therapeutically explore these underlying epigenetic vulnerabilities. Chondrosarcomas demonstrated high sensitivity to histone deacetylase (HDAC) inhibition in both 2D and 3D *in vitro* models, independent of the *IDH* mutation status or the chondrosarcoma subtype. siRNA knockdown and RNA expression data showed that chondrosarcomas rely on the expression of multiple HDACs, especially class I subtypes. Furthermore, class I HDAC inhibition sensitized chondrosarcoma to glutaminolysis and Bcl-2 family member inhibitors, suggesting that HDACs define the metabolic state and apoptotic threshold in chondrosarcoma. Taken together, HDAC inhibition may represent a promising targeted therapeutic strategy for chondrosarcoma patients, either as monotherapy or as part of combination treatment regimens.

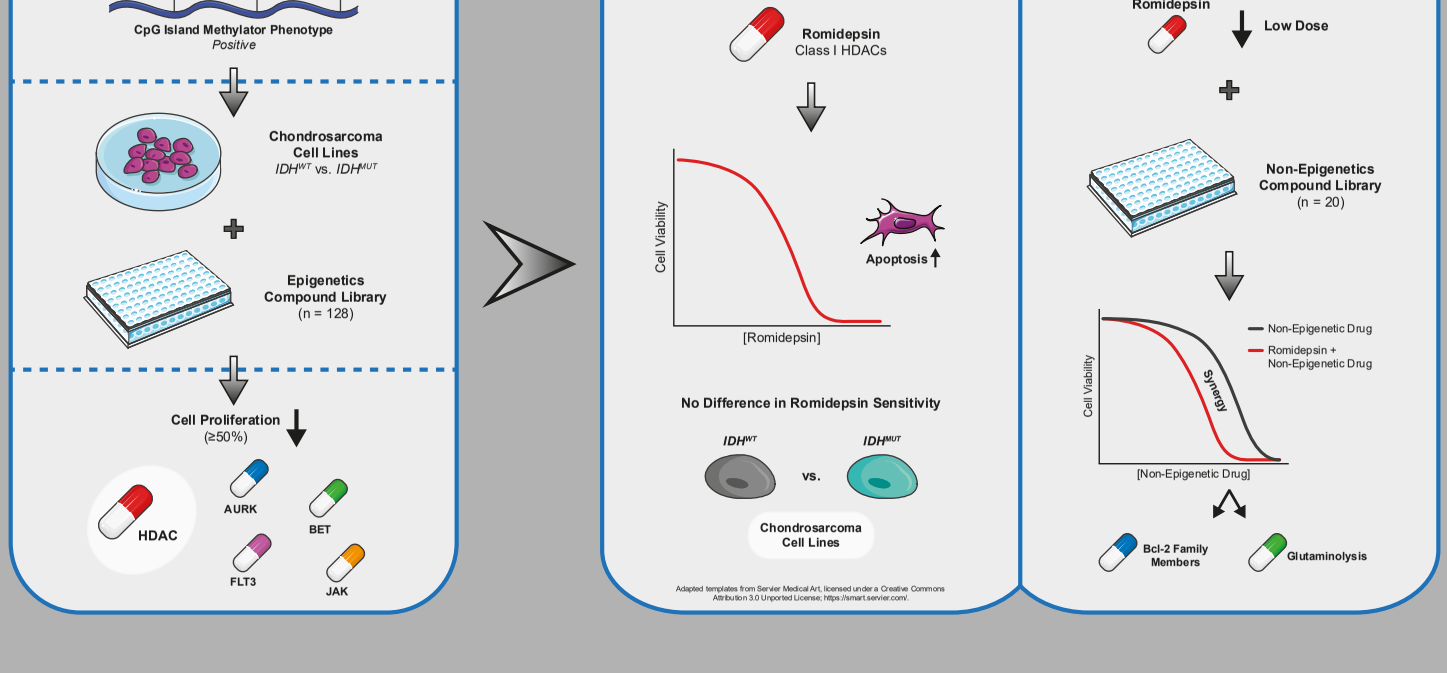
IDH^MUT → Epigenetic Changes
CpG Island Methylator Phenotype
Positive
Chondrosarcoma Cell Lines
IDH^WT vs. IDH^MUT
Epigenetics Compound Library
(n = 128)
Cell Proliferation
(≥50%)
HDAC
AURK
BET
FLT3
JAK
Monotherapy
Romidepsin
Class I HDACs
Cell Viability
[Romidepsin]
Apoptosis
No Difference in Romidepsin Sensitivity
IDH^WT
vs.
IDH^MUT
Chondrosarcoma Cell Lines
Adapted templates from Servier Medical Art, licensed under a Creative Commons Attribution 3.0 Unported License; https://smart.servier.com/.
Combination Therapy
Romidepsin
Low Dose
Non-Epigenetics Compound Library
(n = 20)
Cell Viability
Synergy
Non-Epigenetic Drug
Romidepsin + Non-Epigenetic Drug
[Non-Epigenetic Drug]
Bcl-2 Family Members
Glutaminolysis

Introduction

Chondrosarcomas are bone malignancies characterized by the production of cartilage and account for 20% of all malignant bone tumors [1, 2]. Based on the anatomical location and pathological characteristics of the tumors, chondrosarcomas are divided into several subtypes: conventional chondrosarcoma (85%), dedifferentiated chondrosarcoma (10%), and rare subtypes (5%), which include mesenchymal-, clear cell-, and periosteal chondrosarcomas. Conventional chondrosarcomas are classified into central (85%) and peripheral (15%) tumors, based on their anatomical location (medulla or surface of the bone, respectively) [1, 2]. The most important factor to predict metastatic potential and overall survival of patients with conventional chondrosarcoma is histological grading, which is defined by the cellularity and matrix formation of the tumor. Patients with atypical cartilaginous tumor (ACT)/chondrosarcoma grade I have a low metastatic rate and an overall 10-year survival rate of 88–95% [1, 3]. However, patients with high-grade tumors (i.e., grade II and grade III) have an increased metastasis rate (10% and 71%, respectively) and a decreased overall 10-year survival rate (58–86% and 26–55%, respectively) [2, 3]. This worse prognosis can partially be ascribed to the intrinsic chemo- and radiotherapy resistance of chondrosarcomas and the lack of targeted therapeutic options. Currently, the only curative treatment option for chondrosarcoma patients is surgery [4], which underlines the need to develop novel targeted therapeutic strategies, in particular for patients with unresectable or high-grade tumors.

The most common genetic alteration in central conventional chondrosarcoma is the hotspot mutation affecting the arginine residues encoded by the isocitrate dehydrogenase 1 and -2 (*IDH1* or *IDH2,* collectively referred to as *IDH*) genes (R132 and R140/R172, respectively), occurring in ~50% of the cases [5, 6]. The IDH2 enzyme metabolizes isocitrate to α-ketoglutarate (α-KG) and CO_2 in the tricarboxylic acid cycle, while the IDH1 enzyme is located in the cytosol where it performs a similar reaction. The hotspot mutations induce a gain-of-function of these enzymes, resulting into abnormal cellular concentrations of the oncometabolite D-2-hydroxyglutarate (D-2-HG) [7]. Chondrosarcomas produce relatively high levels of D-2-HG: approximately 40% of the chondrosarcomas harbor an $IDH1^{R132C}$ mutation, which is one of the most efficient D-2-HG producers [8, 9].

Due to the high structural similarity between α-KG and its antagonist D-2-HG, α-KG dependent enzymes are inhibited by the high levels of the oncometabolite [10, 11], causing widespread changes in the metabolic state, DNA damage repair mechanisms, and growth signaling pathways [12, 13]. The epigenetic landscape of *IDH* mutated cells is highly altered due to this competitive inhibition of α-KG dependent DNA demethylases (family of TET enzymes) and histone demethylases (family of Jumonji enzymes) [10, 13],

leading to an aberrant methylation pattern. This indicates that *IDH* mutations interfere with the dynamic processes that regulate the accessibility of the DNA and could thereby permanently change gene expression, which could ultimately lead to tumor formation and growth. Indeed, the introduction of an *IDH* mutation induces the formation of benign cartilage tumors (i.e., enchondromas) in mice [14]. *IDH* mutated enchondromas, which are considered as the benign pre-cursor lesions of chondrosarcoma, are characterized by a CpG island methylator phenotype (CIMP)-positive status [6]. The mutation shifts the differentiation of mesenchymal stem cells, the presumed cells-of-origin in cartilage tumors, towards the chondrogenic lineage [15, 16]. Together, these findings indicate that the *IDH* mutation is an early genetic event which highly alters the epigenetic landscape in early phases of cartilage tumor formation. The characteristic hypermethylation phenotype is also observed in primary *IDH* mutant chondrosarcomas [17]. Therefore, targeting the epigenetic changes induced by *IDH* mutations might be beneficial for chondrosarcoma patients, and could potentially help to overcome the intrinsic chemotherapy resistance in chondrosarcoma.

In this study, we confirmed that the hypermethylation phenotype is retained upon progression from *IDH* mutant enchondroma towards chondrosarcoma using a methylation array on primary tumor samples. In fact, high grade tumors demonstrated an increased number of hypermethylated genes as compared to low grade tumors, suggesting that epigenetic mechanisms play an important role in chondrosarcoma progression. Therefore, a broad compound screen containing 128 compounds which target different epigenetic key players (including histone deacetylases (HDACs), sirtuins (SIRTs), histone demethylases (HDMs), histone acetyltransferases (HATs), histone methyltransferases (HMTs), and DNA methyltransferases (DNMTs)) was performed on *IDH* wildtype and mutant chondrosarcoma cell lines to explore whether these epigenetic changes can be used as a target for novel anticancer therapy. No synthetic lethal interactions with *IDH* mutations were identified, but several general interesting targets were determined, and interesting compound classes included HDAC and bromodomain and extra-terminal motif (BET) protein inhibitors. Additionally, we explored if one of the most promising hits, the HDAC inhibitor romidepsin, could help to sensitize chondrosarcoma cells to chemotherapy or small molecule inhibitors. To address this question, a drug screen with a panel of non-epigenetic drugs was designed to explore if a combination treatment could be a promising therapeutic strategy for chondrosarcoma patients.

Materials and methods

DNA methylation array

Fresh-frozen tumor samples of 20 subjects with solitary benign, low-grade or high-grade cartilage tumors (Table S1) were collected at the LUMC. All samples were handled and coded according to the "Code for Proper Secondary Use of Human Tissue in The Netherlands" (Dutch Federation of Medical Scientific Societies), and their use was approved by the LUMC ethical committee (B17.039). Genomic DNA was isolated with the Wizard Genomic DNA Purification Kit (Promega) according to the manufacturer's protocol. The *IDH* mutation status (Table S1) was confirmed with Sanger sequencing as previously described [6]. Bisulfite conversion of genomic DNA and the Infinium HumanMethylation450 BeadChip array (Illumina, San Diego, CA, USA) were performed as previously described [18]. CIMP-status of all samples was determined as previously described [6]. Hierarchical clustering was based on the 2000 most variable CpG sites and performed with the Ward's method. Differentially methylated genes between benign/low-grade and high-grade samples were determined with a global test [19] after Beta MIxture Quantile dilation (BMIQ) normalization [20]. To identify enriched pathways in the differentially methylated gene sets, the ensemble gene set enrichment analyses (EGSEA) was used [21].

Compounds

Detailed lists of all 128 compounds included in the epigenetics compound library (L1900, Selleckchem, Houston, TX, USA) and of all twenty compounds included in the custom designed compound library for the HDAC inhibitor combination drug screen are available in the supplementary files (Table S3 and Table S4, respectively). The IDH1 mutant (R132H and R132C) inhibitor AGI-5198 (14624, Cayman Chemical, Ann Arbor, MI, USA), the cell permeable derivative of D-2-HG ((2R)-Octyl-α-hydroxyglutarate, 16366, Cayman Chemical), the HDAC inhibitor romidepsin (S3020, Selleckchem), the glutamate dehydrogenase inhibitor chloroquine diphosphate (S4157, Selleckchem), the glutaminase inhibitor metformin HCl (S1950, Selleckchem) and the B-cell lymphoma 2 (Bcl-2) family member inhibitors ABT-737 (Bcl-2/Bcl-xL/Bcl-w, S1002, Selleckchem), S63845 (Mcl-1, S8383, Selleckchem), venetoclax (Bcl-2, S8048, Selleckchem), and WEHI-539 (Bcl-xL, A3935, APExBIO, Houston, TX, USA) were dissolved in DMSO, PBS, or RPMI 1640 medium according to the manufacturer's protocol.

Cell culture

The central conventional chondrosarcoma cell lines CH2879 (*IDH* wildtype (IDH^{WT})) [6, 22], JJ012 ($IDH1^{R132G}$) [6, 23], SW1353 (ATCC, $IDH2^{R172S}$) [6], CH3573 (IDH^{WT}) [24] and L835 ($IDH1^{R132C}$) [6, 25]; the dedifferentiated chondrosarcoma cell lines NDCS1 (IDH^{WT}) [6, 26], HT1080 ($IDH1^{R132C}$) [18, 27], L2975 ($IDH2^{R172W}$) [6, 25] and L3252B (IDH^{WT}) [25]; and the

mesenchymal chondrosarcoma cell line MSC170 (IDH^{WT}) [28] were cultured as described previously [29]. Long-term AGI-5198 treated cell lines (20 passages with 1.5 µM AGI-5198) [18] were cultured in RPMI 1640 medium (Gibco, Invitrogen Life-Technologies, Scotland, UK) supplemented with 10% heat-inactivated fetal bovine serum (FBS) (F7524, Sigma-Aldrich, Saint Louis, MO, USA) and 10µM AGI-5198 (to minimize D-2-HG production). The 3D cell cultures were established and cultured as previously described [30]. All cells were cultured in a humidified incubator with 5% CO_2 at 37 °C. PCR-based mycoplasma tests and STR profiling (GenePrint 10 System, Promega, Madison, WI, USA) were performed regularly.

Primary epigenetics compound screen

The chondrosarcoma cell lines CH2879, JJ012, and SW1353 were seeded in optimized cell densities (5000, 3000, and 3000/well, respectively) in black 96-well plates. After overnight attachment, cells were treated with the epigenetics compound library at a concentration of 2 µM. After 72 h of treatment, cells were fixed with 4% formaldehyde and stained with 2 µg/mL Hoechst 33342 (H1399, Invitrogen Life-Technologies). Plates were imaged using a BD Pathway 855 microscope (BD Biosciences, Breda, The Netherlands) and the number of Hoechst 33342 positive nuclei was quantified using the Image-Pro software (Media Cybernetics, Rockville, MD, USA). All plates were included in the analysis and data were normalized to the negative controls (i.e., PBS and DMSO) to obtain percent of control values. All compounds that reduced the nuclei count ≥50% in at least one of the cell lines were selected for the secondary epigenetics compound screen. The screen was performed in triplicate. A schematic overview of the primary epigenetics compound screen can be found in Figure 2A. A list of all compounds, including the numbering and specific targets, can be found in Table S3.

Secondary epigenetics compound screen

To reduce the D-2-HG levels, *IDH1* mutant cell lines (i.e., JJ012, HT1080, and L835) were pre-exposed to 10 µM AGI-5198 for 72 h [18]. Subsequently, the *IDH1* mutant cell lines were seeded in black 96-well plates (3000, 5000, and 10000/well, respectively) in normal growth medium supplemented with 10µM AGI-5198 or 0.1% DMSO as a control. To mimic D-2-HG production, CH2879 cells were seeded (5000/well) in normal growth medium supplemented with 250 µM D-2-HG or 1% PBS as a control. After overnight attachment, cells were treated with the selected compounds (n = 61) from the primary screen at a concentration of 2 µM. Compounds were diluted in medium supplemented with 0.1% DMSO, 10µM AGI-5198, 1% PBS or 250 µM D-2-HG. After 72 h of treatment, a nuclei count was performed as described under the methods section of the primary epigenetics compound screen. All plates were included in the analysis and data were normalized to the negative controls (i.e., PBS and DMSO) to obtain percent of control values. Compounds that

reduced the nuclei count ≥50% in all cell lines were considered as potential therapeutic options for both *IDH* wildtype and *IDH* mutant chondrosarcomas. A ≥75% difference in nuclei count between cells treated with or without 10 µM AGI-5198 or cells treated with or without 250 µM D-2-HG was considered as a potential synthetic lethal interaction with the *IDH* mutation. The screen was performed in triplicate. A schematic overview of the secondary epigenetics compound screen can be found in Figure 2C.

HDAC inhibitor combination drug screen

CH2879 cells (7000/well), JJ012 cells (3000/well), and SW1353 cells (3000/well) were seeded in 96-well plates in normal growth medium supplemented with 0.1% DMSO or romidepsin (1 nM (JJ012 cells) and 0.75 nM (CH2879 and SW1353 cells)). After overnight attachment, cells were treated with the custom designed compound library. For each library compound, five concentrations were tested, which were based on previous experience (Table S4). Compounds were diluted in normal growth medium supplemented with 0.1% DMSO or romidepsin (0.75 nM or 1 nM) and added to the cells. The solvents DMSO and PBS were used as negative controls and 3.16 nM romidepsin was used as positive control. After 72 h of treatment, cells were fixed with 4% formaldehyde and stained with 2 µg/mL Hoechst 33342. To automatically count the nuclei, the Cellomics ArrayScan VTI HCS 700 series and HCS Studio Cell Analysis Software (ThermoFisher Scientific, Waltham, MA, USA) were used. Plates were excluded from the analysis if a low correlation with the other replicates was observed (R square ≤ 0.8) combined with a Z'-factor < 0.5. Data were normalized to the negative controls (i.e., PBS and DMSO) to obtain percent of control values. A ≥20% difference in nuclei count between cells treated with or without romidepsin was considered as a potential synergistic treatment combination. The screen was performed in triplicate. A schematic overview of the HDAC inhibitor combination drug screen can be found in Figure 5A. A list of all compounds, including the specific targets, can be found in Table S4.

Cell viability and nuclei count assays

For the 2D cell cultures, the cell viability assays, nuclei count assays and data analysis were performed as previously described [29]. Cells were treated for 72 h with tubacin, romidepsin, ABT-737, venetoclax, WEHI-539, S63845, chloroquine diphosphate, or metformin in concentrations ranging from 0.0316 nM to 31.6 mM. Cells treated with DMSO or PBS were used as a negative control. Experiments were performed in triplicate and repeated one to three times.

For the 3D cell cultures, the cell viability assays and the immunohistochemical stains (Ki-67 and cleaved caspase 3) were performed as previously described [30]. Cells were grown in alginate beads for 14 days and subsequently treated for 72 h with romidepsin in

concentrations ranging from 0.1 to 10 nM. Experiments were performed in triplicate and repeated four times.

siRNA transfection

Reverse siRNA transfection was performed for CH2879 cells (10,000/well) and JJ012 cells (5000/well) in 96-well plates. To achieve transient knockdown of all HDAC subtypes, cells were transfected with 0.1 µL/well DharmaFECT 3 (Dharmacon, Lafayette, CO, USA) and 50 nM siRNA SMARTpools (Dharmacon), which consist of four individual siRNAs targeting a gene of interest. The mock condition, the siRNA SMARTpool against Glyceraldehyde-3-Phosphate Dehydrogenase *(GAPDH)* (Dharmacon) and an siKinasePool (a mixture of diluted siRNAs targeting kinases with a final total siRNA concentration of 50 nM) were used as negative controls. siRNA SMARTpools against Kinesin Family Member 11 *(KIF11)* and Polo Like Kinase 1 *(PLK1)* (Dharmacon) were used as positive controls. To reduce toxicity, the medium was refreshed 24 h after the transfection. Three days after medium refreshment, cells were fixed, stained with Hoechst 33342 and imaged with the Cellomics ArrayScan VTI HCS 700. Data were normalized to the negative controls to obtain percent of control values. The experiment was performed in triplicate.

Next-generation RNA sequencing analysis

RNA expression of all HDAC subtypes in chondrosarcoma cell lines was extracted from a next generation RNA sequencing dataset we previously described [18]. Reads per kilobase per million (RPKM) were used to describe gene expression levels.

Apoptosis and cell cycle assays

The apoptosis and cell cycle assays were performed and analyzed as previously described [29]. Cells were treated with 3 nM romidepsin for 24 h and 48 h. In both assays, DMSO was used as a negative control. In the apoptosis assay, 5 µM ABT-737 combined with 1 µM doxorubicin was used as a positive control. Experiments were performed in singular (cell cycle) or duplicate (apoptosis) and repeated three times.

Western blotting

Sample preparation, western blotting and quantification were performed as previously described [29]. Cells were treated with different compounds (i.e., romidepsin, ABT-737, and venetoclax) for 24 h to 72 h in concentrations ranging from 0.316 nM to 10 µM. Western blots were stained for the expression of full-length/cleaved caspase 3 (1:1000, 8G10, Cell Signaling Technology (CST), Leiden, The Netherlands), full-length/cleaved PARP (1:1000, 46D11, CST), acetyl-Histone H3 (Lys9) (acH3K9) (1:1000, clone C5B11, CST), Mcl-1 (1:1000, #4572, CST), Bcl-xL (1:1000, 54H6, CST), Bcl-2 (1:1000, D55G8, CST), Bcl-w (1:1000, 31H4, CST), Bak (1:1000, D4E4, CST), Bim (1:1000, C34C5, CST), Bid (1:1000, #2002, CST), and Bax

(1:1000, D2E11, CST). α-Tubulin (1:30,000, DM1A, Sigma-Aldrich) was used as a loading control.

Statistical analysis

To determine significant changes between experimental groups, a nonparametric Kruskal–Wallis test followed by a Dunn's post-hoc test was performed. A Grubbs' test was performed to detect outlier values in the dose–response curve datasets. All statistical tests were performed in GraphPad Prism 8. The Z'-factor was used as a measure for compound screen quality and was calculated to determine the effect size between negative and positive controls [31]. To calculate synergy in combined drug treatments, the Bliss independence model was used [32, 33]. Heatmap figures were created with the online tool MORPHEUS (Broad Institute, Cambridge, MA, USA).

Results

IDH mutant chondrosarcomas have increased hypermethylation with increasing histological grade

CIMP-status analysis shows that almost all *IDH* mutant cartilage tumors were CIMP-positive, except for one enchondroma and one low-grade chondrosarcoma (L533 and L1769, respectively) (Figure 1A, Table S1). Hierarchical clustering of the methylome of these 20 *IDH* mutant primary cartilage tumors resulted in two clusters: a group dominated by benign/low-grade cartilage tumors and a group consisting of solely high-grade chondrosarcomas (Figure 1A). Thus, even though all tumors contained a mutation in *IDH*, and most of them were CIMP-positive, the methylation status was strongly influenced by the histological grade. When comparing the two groups, it turned out that high-grade tumors were more strongly methylated for 592 genes, while they were less strongly methylated for 89 genes (Figure 1B; gene lists are shown in Table S2). Of note, grade III chondrosarcomas were even more strongly methylated than grade II chondrosarcomas (Figure S1A). Biological pathway analysis showed that especially signal transduction and inflammation related genes were affected by increased promoter methylation (Figure S1B). Hence, epigenetic mechanisms seem to play an important role in chondrosarcoma progression. To further explore these underlying epigenetic vulnerabilities, we took a screening-based approach to identify epigenetic regulators that play a role in high-grade chondrosarcoma.

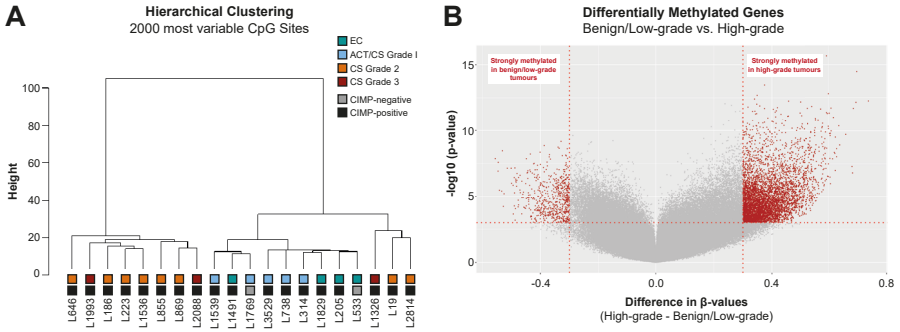

Figure 1. *IDH* mutant chondrosarcomas have increased hypermethylation with increasing histological grade. **(A)** Hierarchical clustering of the methylome of *IDH* mutant primary cartilage tumors (n = 20) showed a cluster dominated by benign/low-grade cartilage tumors and a cluster of solely high-grade tumors. Almost all tumors had a CIMP-positive status. Clustering was based on the 2000 most variable CpG sites and performed with the Ward's method. EC: enchondroma, ACT: atypical cartilaginous tumor, CS: chondrosarcoma. **(B)** Volcano plot of differentially methylated genes between benign/low-grade and high-grade cartilage tumors. Vertical red lines indicate a difference in β-values of at least 0.3 between the two groups. Significantly differentially methylated genes are indicated with red (cut-off at $p < 0.001$). A gene list can be found in Table S2.

Epigenetic compound screening identifies HDAC enzymes as important epigenetic regulators in chondrosarcoma, independent of the *IDH* mutation status

The primary epigenetics compound screen was performed as described in Figure 2A. The results show that several compound classes reduced the growth of all chondrosarcoma cell lines, including Aurora kinase inhibitors, BET protein inhibitors, Fms Related Receptor Tyrosine Kinase 3 (FLT3) inhibitors, HDAC inhibitors, and Janus kinase (JAK) inhibitors (Figure 2B). Of note, DNA methyltransferase (DNMT) inhibitors did not have a pronounced effect on chondrosarcoma cell growth, except for #27 (decitabine). All compounds that inhibited growth with ≥50%, as indicated by the bold numbers in Figure 2B, were selected for the secondary epigenetics compound screen (Figure 2C).

The secondary screen identified 17 compounds that reduced cell growth with ≥50% in all five chondrosarcoma cell lines, among which the HDAC inhibitors represented the biggest group (Figure 2D). Furthermore, the secondary screen showed that the effect of the compounds seemed independent of the *IDH* mutation status, as only one potential synthetic lethal interaction was observed in JJ012 cells (#65, tubacin) (Figure S1A). However, dose–response curves of tubacin in *IDH1* mutant cell lines treated with or without the IDH1 mutant inhibitor AGI-5198 [34] did not confirm the rescue observed in the secondary epigenetics compounds screen (Figure S2B). Hence, these results suggest that targeting of epigenetic regulators in chondrosarcoma, especially the HDAC enzymes, could be a promising therapeutic strategy, irrespective of the *IDH* mutation status.

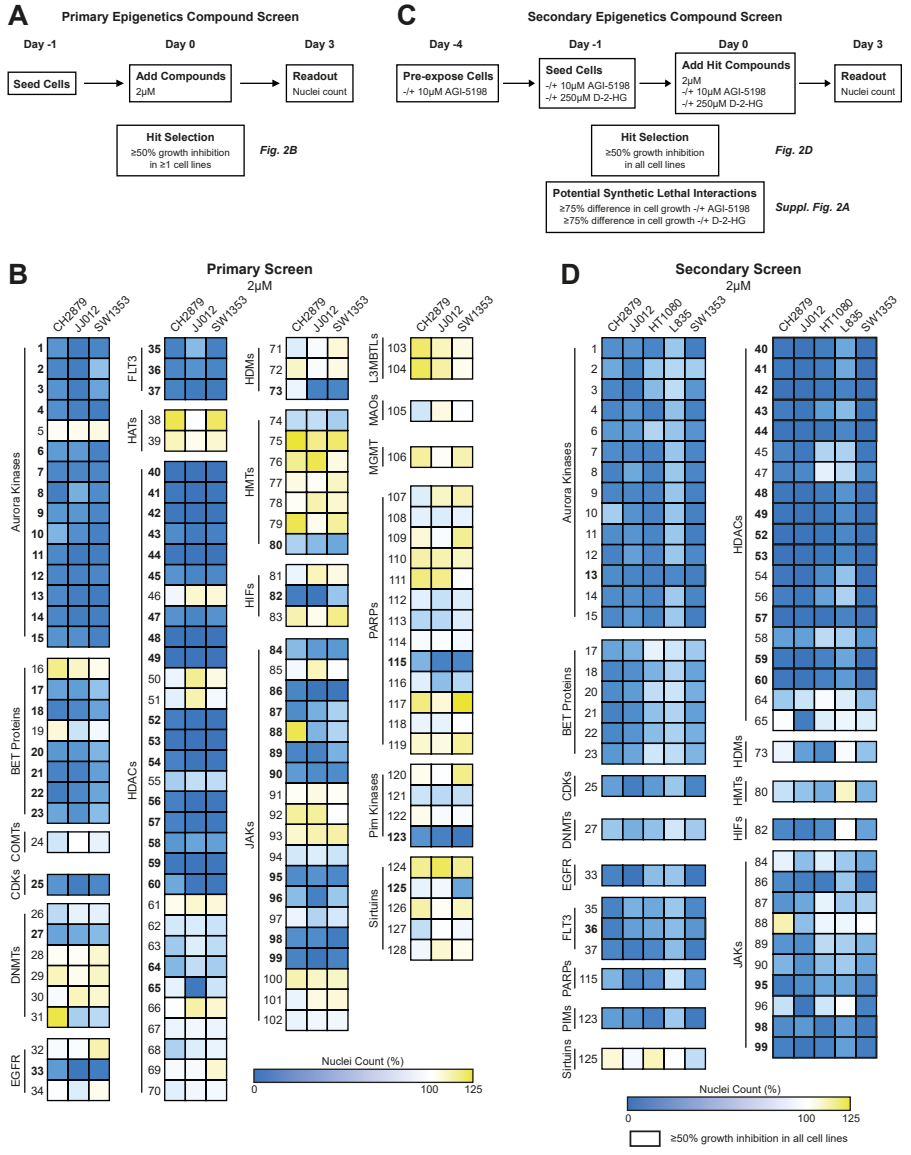

Figure 2. Drug screening identifies HDAC enzymes as important epigenetic regulators in chondrosarcoma, independent of the *IDH* mutation status.

(A) Schematic overview of the performed primary epigenetics compound screen. **(B)** Heatmaps of the results from the primary epigenetics compound screen, in which blue indicates inhibition of cell growth and yellow an induction of cell growth. Three chondrosarcoma cell lines were treated with 128 compounds at a concentration of 2 μM for 72 h. Aurora kinase, BET protein, FLT3, HDAC, and JAK inhibitors were identified as interesting compound classes. All compounds (n = 61) that inhibited growth ≥50%, indicated by the bold numbers, were selected for the secondary screen. **(C)** Schematic overview of the performed secondary epigenetics compound screen. **(D)** Heatmaps of the results from the secondary epigenetics compound screen. Five chondrosarcoma cell lines were treated with 61 compounds at a concentration of 2 μM for 72 h. All compounds that reduced the nuclei count ≥50% in all cell lines were identified as hit (n = 17). HDAC inhibitors were identified as the most promising compound class (n = 12).

Chondrosarcoma cell lines mainly rely on the expression of HDAC class I subtypes

The human genome encodes for eleven subtypes of HDAC enzymes, which can be divided into four different classes: class I (HDAC1, -2, -3, and -8), class IIA (HDAC4, -5, -7, and -9), class IIB (HDAC6 and HDAC10), and class IV (HDAC11). To identify the most potent and specific HDAC inhibitor for follow-up studies, all HDAC inhibitors were screened at a lower concentration (i.e., 0.2 μM) and ordered based on HDAC class specificity (Table S3). As shown in Figure 3A, chondrosarcoma cell lines were sensitive to HDAC inhibitors that target multiple classes. Interestingly, one specific class I HDAC inhibitor (i.e., romidepsin) reached a similar level of growth inhibition in all cell lines as some pan-HDAC inhibitors. To evaluate if one of the eleven HDAC subtypes plays the most pivotal role in chondrosarcoma cell survival, siRNA knockdown for each subtype was performed in CH2879 and JJ012 cell lines. Knockdown of a single HDAC subtype did not have a prominent effect on chondrosarcoma cell line growth (Figure 3B), which suggests that chondrosarcoma cell lines rely on multiple HDAC subtypes to maintain cellular growth. Of note, knockdown of the class I subtypes HDAC1 and HDAC2 had the most pronounced effect on the growth of CH2879 cells and JJ012 cells, respectively (Figure 3B). Additionally, analysis of previously published RNA sequencing data [18] showed that chondrosarcoma cell lines expressed all 11 HDAC subtypes, among which class I was most abundantly expressed (Figure 3C). Overall, this data indicates that multiple HDAC subtypes play a pivotal role in chondrosarcoma cell growth and highlights class I as the most important subgroup. Therefore, the class I HDAC inhibitor romidepsin was selected for further validation studies.

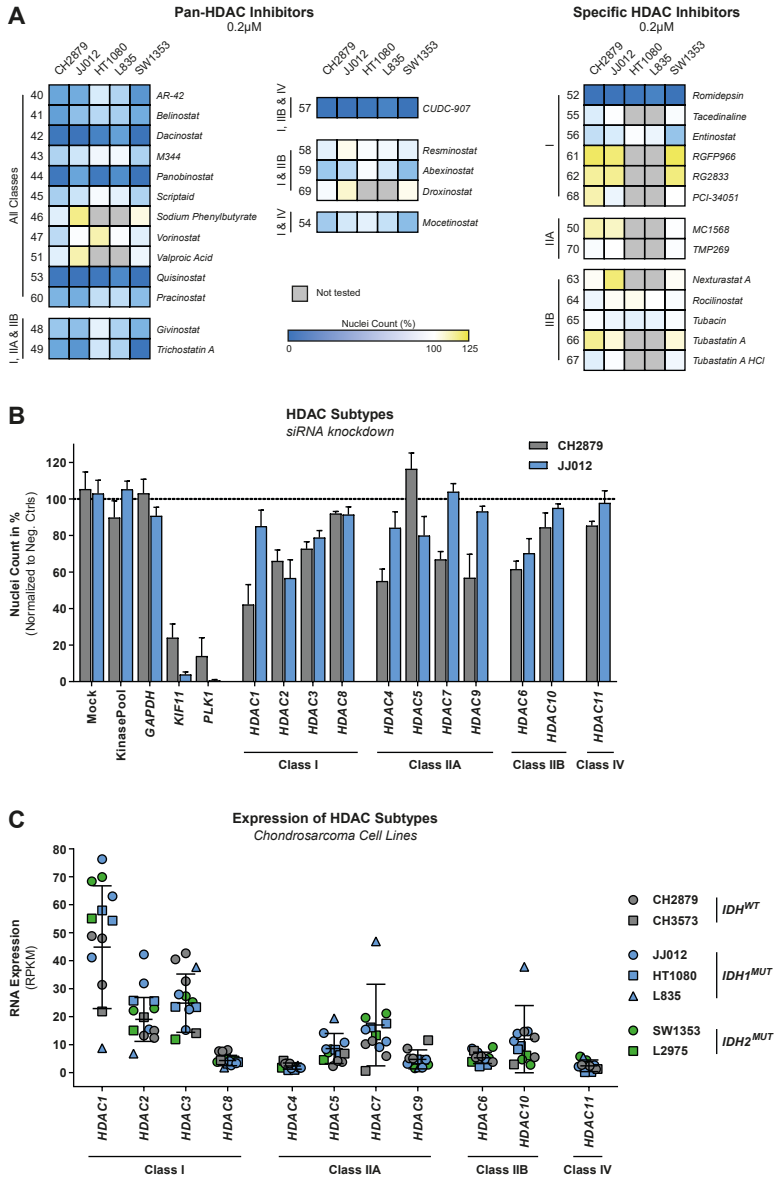

Figure 3. Chondrosarcoma cell lines mainly rely on the expression of HDAC Class I subtypes.
(A) Heatmap that visualizes the results of five chondrosarcoma cell lines which were treated with all HDAC inhibitors included in epigenetics compound screen (*n* = 31) at a concentration of 0.2 µM for 72 h. Blue indicates inhibition of cell growth and yellow an induction of cell growth. Grey indicates that an inhibitor was not tested in that specific cell line. Inhibitors were sorted on the specific HDAC classes that are targeted by these compounds. Chondrosarcoma cell lines are sensitive to several pan-HDAC inhibitors and the selective class I HDAC inhibitor romidepsin. **(B)** Knockdown of all single HDAC subtypes with siRNA SMARTpools and DharmaFECT 3 in two chondrosarcoma cell lines did not have a prominent effect on chondrosarcoma cell line growth. Mock, siGAPDH, and siKinasePool were used as negative controls, and siKIF11 and siPLK1 were used as positive controls. Bars represent the mean of one experiment performed in triplicate ± standard deviation. **(C)** RNA expression of all HDAC subtypes per cell line determined from a previously published RNA sequencing data set [18]. Class I HDAC subtypes were most abundantly expressed in chondrosarcoma cell lines.

Chondrosarcoma cell lines are sensitive to romidepsin, irrespective of the chondrosarcoma subtype or *IDH* mutation status

Romidepsin is clinically approved for the treatment of cutaneous T-cell lymphoma and other peripheral T-cell lymphomas, and is highly selective for binding class I subtypes as compared to the other HDAC classes [35, 36]. Dose–response curves showed that all chondrosarcoma cell lines were highly sensitive to romidepsin with GR_{50} values in the range of 0.89 to 1.96 nM after 72 h of treatment (Figure 4A and Table 1). The response to romidepsin treatment was independent of chondrosarcoma subtype and the *IDH* mutation status, as the effect could not be rescued if JJ012 was treated long-term with AGI-5198 (Figure 4A and Table 1). Furthermore, dose–response curves of romidepsin in 3D cell cultures of CH2879, JJ012, and SW1353 showed similar IC_{50} values as compared to the values obtained in the 2D cell culture experiments (Figure 4B and Table 1).

Table 1. IC_{50} and growth corrected values (i.e., GR_{50}) of 72 h romidepsin treatment in chondrosarcoma cell lines.

Cell Line	Subtype	*IDH* Status	2D Cell Culture		3D Cell Culture
			GR_{50} (nM)	IC_{50} (nM)	IC_{50} (nM)
MCS170	Mesenchymal	Wildtype	0.89	2.69	-
L835	Central conventional	*IDH1* R132C	0.97	29.2	-
JJ012 + AGI-5198	Central conventional	*IDH1* R132G (inhibited)	1.06	0.96	-
SW1353	Central conventional	*IDH2* R172S	1.10	1.01	2.00
HT1080	Dedifferentiated	*IDH1* R132C	1.10	0.99	-
CH3573	Central conventional	Wildtype	1.26	1.37	-
L2975	Dedifferentiated	*IDH2* R172W	1.27	1.29	-
L3252B	Dedifferentiated	Wildtype	1.30	1.51	-
CH2879	Central conventional	Wildtype	1.79	1.61	2.96
NDCS1	Dedifferentiated	Wildtype	1.92	1.57	-
JJ012	Central conventional	*IDH1* R132G	1.96	1.71	5.08

To assess the underlying cell death mechanism, three chondrosarcoma cell lines (i.e., CH2879, JJ012, and SW1353) were treated with a high dose of romidepsin (i.e., 3 nM) for 24 h or 48 h. Caspase 3/7 activity was significantly induced in SW1353 cells after 24 h, and in all cell lines after 48 h (Figure 4C). A concomitant significant decrease in the viability of JJ012 and SW1353 cells was also observed after 48 h of treatment (Figure 4C). A western blot for cleaved PARP and cleaved caspase 3 confirmed the observed induction of apoptosis (Figure 4D). An increase in apoptosis as well as a reduction in proliferation were also observed in the 3D cell culture models (Figure S3). Cell cycle analysis showed that romidepsin treatment caused a cell cycle arrest in either the G2/M phase for CH2879 or both the G1 phase (24 h) and G2/M phase (48 h) for JJ012 (Figure 4E). Hence, these data indicate that romidepsin could be further explored *in vivo* as a promising therapeutic strategy for chondrosarcoma, irrespective of the chondrosarcoma subtype and the *IDH* mutation status.

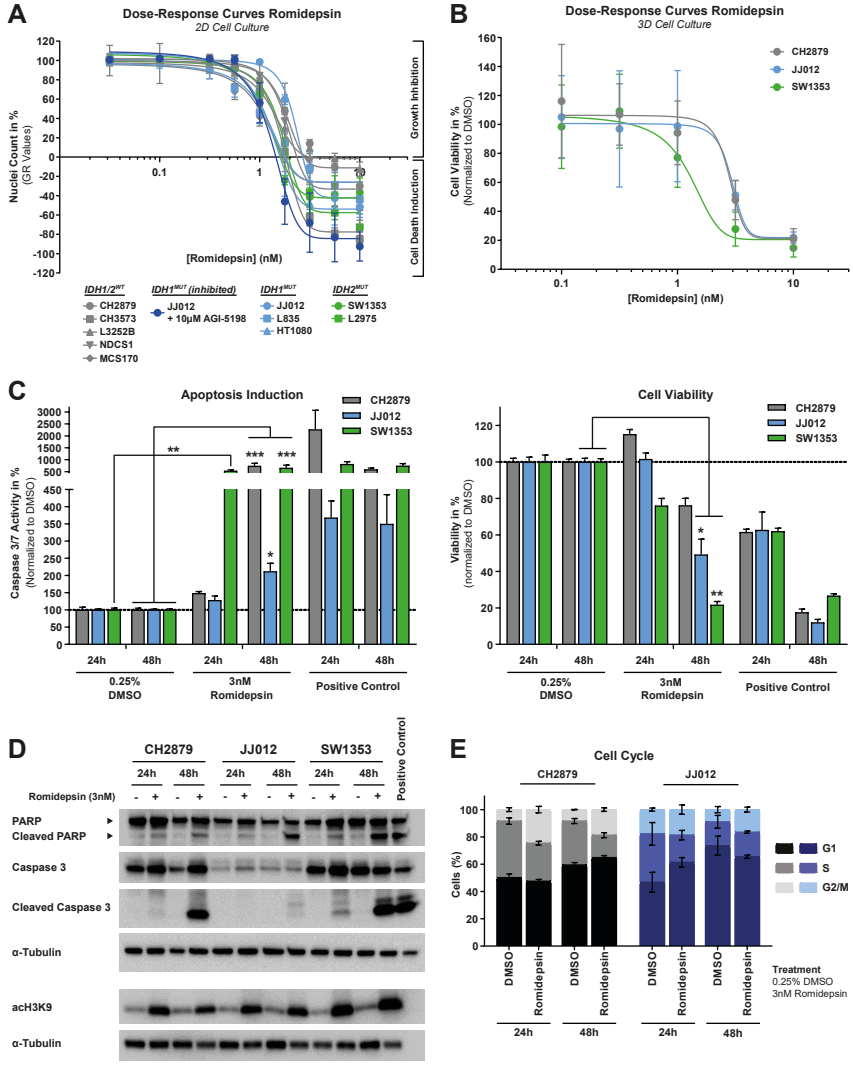

Figure 4. Romidepsin inhibits growth, induces apoptosis and causes a cell cycle arrest in chondrosarcoma cell lines. **(A)** Dose–response curves of romidepsin after 72 h of treatment for 10 chondrosarcoma cell lines cultured in 2D. Chondrosarcoma cell lines were highly sensitive to romidepsin treatment, and the effect could not be rescued if the JJ012 cell line was treated long-term with 10 µM AGI-5198 (>20 passages). Data were corrected for growth rate (GR values) and GR_{50} values were calculated. Data points represent the mean of three experiments performed in triplicate ± standard deviation. **(B)** Dose–response curves of romidepsin after 72 h of treatment for three chondrosarcoma cell lines cultured in 3D. Romidepsin sensitivity was comparable between 2D and 3D culture conditions. Data points represent the mean of four experiments performed in triplicate ± standard deviation. **(C)** Cleaved caspase 3/7 activity and corresponding viability after 24h and 48 h treatment with 3 nM romidepsin. All cell lines showed a significant increase in apoptosis after 48 h of treatment. As a positive control, treatment with 5µM ABT-737 + 1µM doxorubicin was used. Bars represent the mean of three experiments performed in duplicate ± standard deviation. Significant changes were determined with a Kruskal–Wallis/Dunn's test: * = $p < 0.05$, ** = $p < 0.01$, *** = $p < 0.001$, **** = $p < 0.0001$. **(D)** Western blot for full-length/cleaved PARP, full-length/cleaved caspase 3 and acH3K9 after 24 h and 48 h treatment with 3 nM romidepsin. All cell lines showed an induction in histone H3 acetylation and apoptosis after 24 h or 48 h of treatment, respectively. As a positive control for apoptosis induction, CH2879 cells treated for 24 h with 5µM ABT-737 + 1µM doxorubicin were used. α-Tubulin was used as a loading control. Whole blots with densitometry readings can be found in Figure S7A. **(E)** Cell cycle analysis after 3 nM romidepsin treatment for 24 h or 48 h. Romidepsin caused a G1 or G2/M phase cell cycle arrest, depending on the time-point and cell line. Bars represent the mean of three independent experiments ± standard deviation.

HDAC inhibitor combination drug screen identifies Bcl-2 family member inhibitors and metabolic compounds as potential combination treatment strategies

As HDAC inhibitors induce the acetylation of histones, the level of acetylated histone 3 (acH3K9) was determined after 24 h and 48 h treatment with romidepsin. An induction of acH3K9 was observed in all three chondrosarcoma cell lines (Figure 4D). However, this high dose of romidepsin highly affects the cellular growth of these chondrosarcoma cell lines after 72 h (Figure 4A). Lower dosages of romidepsin also showed a prominent induction of acH3K9 (0.75 nM for CH2879 and SW1353 cells and 1 nM for JJ012 cells), whilst the effect on cellular growth was minimal (> 80% nuclei left after 72 h) (Figure S4). These results indicate that low dosages of romidepsin induce changes in epigenetic landscape of chondrosarcoma cells, and these sub-optimal romidepsin dosages could be used to sensitize chondrosarcoma cells to non-epigenetic treatments such as chemotherapy and small molecule inhibitors.

Twenty non-epigenetic drugs were selected for the HDAC inhibitor combination drug screen (Table S4). These drugs either have a known synergistic effect with HDAC inhibitors (e.g., chemotherapy and proteasome inhibitors [37]) or were previously successful as single agent in chondrosarcoma cell lines (e.g., PARP and NAMPT inhibitors [29, 38]). A schematic overview of the combination drug screen can be found in Figure 5A. As a screen quality control, the induction of acH3K9 was determined by western blot (Figure 5B). Addition of romidepsin sensitized three chondrosarcoma cell lines to 6 out of 20 non-epigenetic drugs: four Bcl-2 family member inhibitors and two metabolic compounds (Figure 5C). The other 14 compounds did not show a beneficial effect when combined with HDAC inhibition, except for CB-839 treatment in CH2879 cells and sapanisertib treatment in SW1353 cells (Figure S5).

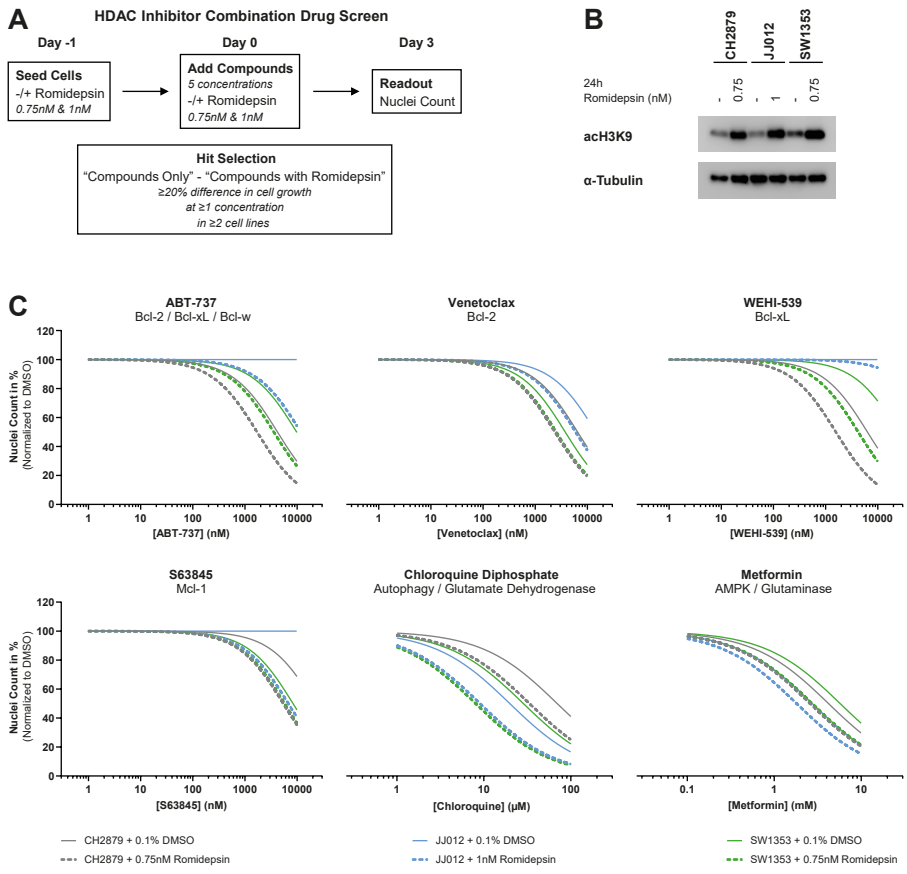

Figure 5. Low dose of romidepsin sensitizes chondrosarcoma cell lines to several non-epigenetic drugs.
(A) Schematic overview of the performed HDAC inhibitor combination drug screen. **(B)** Western blot for acH3K9 after 24 h treatment with low doses of romidepsin. Histone 3 acetylation was induced in the HDAC inhibitor combination drug screen. α-Tubulin was used as a loading control. Whole blots with densitometry readings can be found in Figure S7B. **(C)** Dose–response curves of the six most promising combination therapies identified in the HDAC inhibitor combination drug screen. Three chondrosarcoma cell lines were treated with twenty non-epigenetic drugs in five concentrations (72 h) with or without romidepsin (96 h). A difference in nuclei count of ≥20% between –/+ romidepsin conditions was considered as a potential synergistic treatment combination. Graphs represent the normalized non-linear fit which was calculated based on the individual data points (not shown).

Romidepsin sensitizes chondrosarcoma cells to Bcl-2 family member inhibitors and affects the expression of both anti- and pro-apoptotic proteins

The general Bcl-2 family member inhibitor, ABT-737, and the specific Bcl-2 inhibitor, venetoclax, showed the highest synergistic effect when combined with romidepsin, especially at higher drug concentrations (Figure 6A-B, Figure S6). Induction of apoptosis due to these combination treatments was confirmed by the expression of cleaved PARP and cleaved caspase 3 in both CH2879 and JJ012 cells, but apoptotic cell death was less pronounced in SW1353 cells (Figure 6C). To understand the underlying mechanism, the protein expression of anti- and pro-apoptotic Bcl-2 family members was determined after 24 h to 48 h treatment with a low dose of romidepsin. The expression of all anti-apoptotic family members was downregulated after 48 h of treatment, except for Bcl-w expression in CH2879 cells (Figure 6D). In contrast, the expression of pro-apoptotic proteins was either up- or downregulated after 48 h treatment with low dosages of romidepsin, depending on the pro-apoptotic protein subtype and chondrosarcoma cell line (Figure 6D). Hence, these results indicate that HDAC inhibition can change the balance between pro- and anti-apoptotic proteins, which could explain why the combination treatment with HDAC inhibition and Bcl-2 family member inhibition is highly synergistic in chondrosarcoma cells.

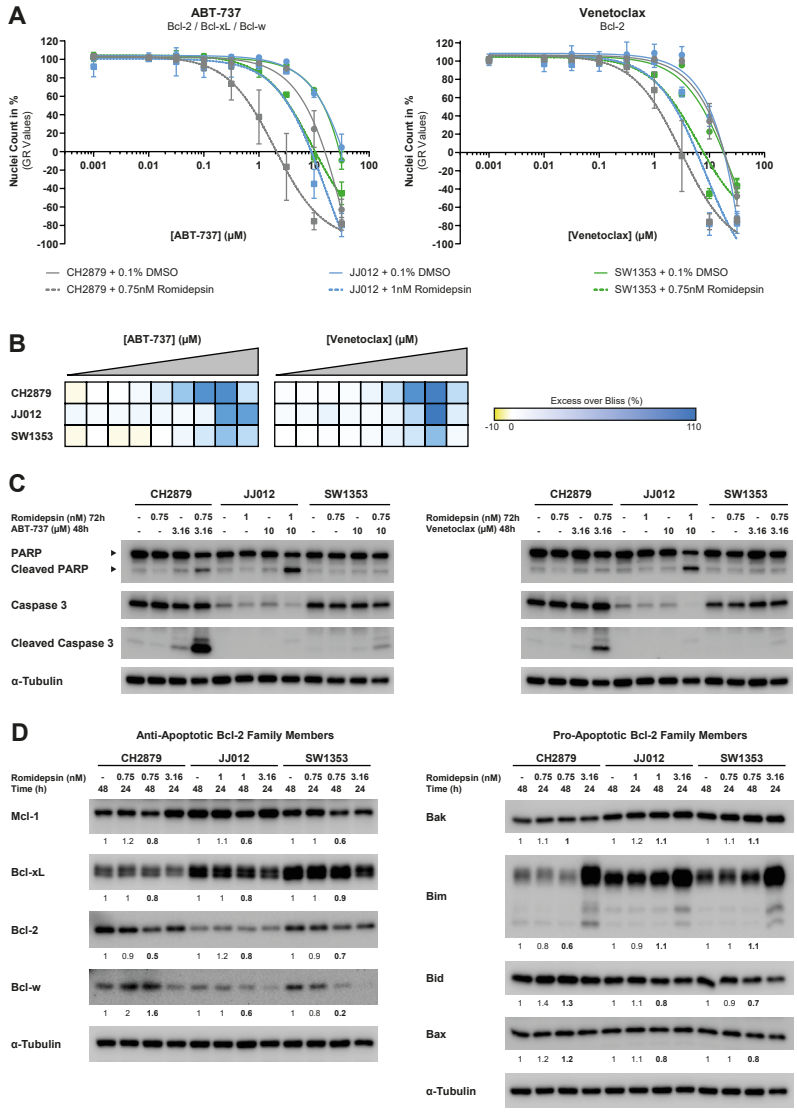

Figure 6. Romidepsin sensitizes chondrosarcoma cells to Bcl-2 family member inhibitors and affects the expression of both anti- and pro-apoptotic proteins.
(A) Dose–response curves of single or combination treatment strategies after 72 h of treatment for three chondrosarcoma cell lines. Romidepsin sensitized chondrosarcoma cell lines to both ABT-737 and venetoclax treatment. Data were corrected for growth rate (GR values). Data points represent the mean of two experiments performed in triplicate ± standard deviation. **(B)** Heatmaps of the calculated Excess over Bliss scores for the combination treatment strategies. Yellow represents antagonism, white represents additivity and blue represents synergy. Combination treatment strategies were synergistic when high concentrations of ABT-737 and venetoclax were used. **(C)** Western blots for full-length/cleaved PARP and full-length/cleaved caspase 3 after single or combined treatment with romidepsin (72 h) and/or ABT-737/venetoclax (48 h). Combination treatment strategies induced more apoptosis than single agent treatment strategies. α-Tubulin was used as a loading control. Whole blots with densitometry readings can be found in Figure S7C. **(D)** Western blots for anti-apoptotic and pro-apoptotic Bcl-2 family members after 24 h and 48 h treatment with low doses of romidepsin (0.75 nM or 1 nM). Low romidepsin doses affected the expression of both anti- and pro-apoptotic Bcl-2 family members. As a positive control, 24 h treatment with a high dose of romidepsin (3.16 nM) was used. α-Tubulin was used as a loading control. For each sample, expression of Bcl-2 family members was normalized to α-tubulin expression. For each cell line, fold changes were calculated relative to the untreated control. Whole blots with densitometry readings can be found in Figure S7D.

Discussion

In this study, we explored whether the methylome is altered upon progression from *IDH* mutant enchondroma towards chondrosarcoma. We showed that the CIMP-positive status is retained in high-grade *IDH* mutant chondrosarcoma. Moreover, the number of highly methylated genes seemed to increase upon tumor progression. This suggests that methylation patterns change upon chondrosarcoma progression, and that an increased number of methylated genes is associated with aggressiveness of the disease. Since we chose to include a homogeneous *IDH* mutant subgroup of chondrosarcomas, it remains to be established whether methylation is equally important in *IDH* wildtype chondrosarcomas. The epigenetics compound screen results, indicating sensitivity to the same epigenetic modulators, suggest that the epigenetic landscape is comparable between *IDH* mutant and wildtype chondrosarcomas. This is further supported by the lack of a synthetic lethal interaction between the *IDH* mutation and a broad spectrum of epigenetic regulators, even though these kinds of synthetic lethal interactions (i.e., BET protein and DNMT inhibitors) were previously described in *IDH* mutant acute myeloid leukemia (AML) and glioma [39–41]. Together, these data suggest that the epigenetic landscape is highly altered in cartilage tumors, and that these changes go beyond the effect of the *IDH* mutation on the methylome.

Based on the retained CIMP-positive status and the increasing amount of hypermethylated genes in high-grade *IDH* mutant chondrosarcoma tumors, we expected that targeting of DNMTs by for instance decitabine and azacytidine would be effective in chondrosarcoma. However, none of these DNMT inhibitors had a pronounced effect on chondrosarcoma cell viability. Nevertheless, the epigenetics compound screens identified several other classes of interesting drug targets for both *IDH* wildtype and *IDH* mutant chondrosarcoma, among which inhibitors against Aurora kinases, FLT3, HDAC, and JAK showed the most pronounced effect on chondrosarcoma cell growth. Most of these targets play a major role in growth signaling pathways (FLT3 and JAK) or cell cycle control (Aurora kinases). We have previously shown that targeting cell cycle regulators, especially Checkpoint Kinase 1 (CHK1), could be a promising therapeutic strategy for chondrosarcoma patients [42]. Hence, non-epigenetic targets are of interest, but this went beyond the scope of the present study.

The HDAC enzymes play a prominent role in skeletal development and aberrant expression is associated with a wide variety of bone-related abnormalities. HDAC1 and HDAC3 are most abundantly expressed in healthy human cartilage [43], and we showed that these subtypes are also highly expressed in chondrosarcoma cell lines. Of note, the expression of HDAC2, HDAC7, and HDAC10 seemed to be increased in chondrosarcoma cell lines as

compared to healthy human cartilage [43], and romidepsin targets one of these subtypes (i.e., HDAC2). Overexpression of class I HDAC subtypes (HDAC1, -2, -3, and -8) inhibits the expression of cartilage-specific genes (e.g., *COL2A1*), leading to the disruption of normal cartilage development [44], while its inhibition might promote differentiation and reduce proliferation. This mechanism could underlie romidepsin sensitivity in chondrosarcoma but warrants further investigation.

Previously, it was shown by other groups that the HDAC inhibitors romidepsin, trichostatin A, and sodium valproate affect cell proliferation in 2D *in vitro* models of chondrosarcoma [45, 46]. In this study, we found that chondrosarcoma cell lines are highly sensitive to HDAC inhibition in both 2D and 3D *in vitro* models, especially to pan-HDAC inhibitors and the specific class I HDAC inhibitor romidepsin. Moreover, we showed that sensitivity to romidepsin is independent of the *IDH* mutation status and the chondrosarcoma subtype (i.e., central conventional-, dedifferentiated-, or mesenchymal chondrosarcoma), indicating that HDAC inhibition could be a promising therapeutic strategy for all chondrosarcoma patients. Romidepsin is clinically approved for the treatment of cutaneous T-cell lymphoma and other peripheral T-cell lymphomas. *In vitro* studies of romidepsin treatment in T-cell lymphomas report IC_{50} values in the low nanomolar range (1 to 11 nM) [47, 48], which are comparable to the determined GR_{50} and IC_{50} values in our 2D and 3D chondrosarcoma cell culture models. The currently approved dosing regimen of romidepsin in patients with T-cell lymphomas reaches maximum plasma concentrations of 700 nM [49], which further supports that our findings are not related to off-target and toxic side effects. Moreover, romidepsin significantly reduces tumor growth in a subcutaneous chondrosarcoma mouse model [45]. Additional research in an orthotopic chondrosarcoma mouse model [50] should be performed to confirm the efficacy of romidepsin in an *IDH* mutation status independent manner. As *in vitro* and *in vivo* models differ in nutrient availability, metabolism and cell types involved in tumor growth, the downstream effects of *IDH* mutations on the epigenetic landscape and the metabolism might also vary between these two types of models.

We also explored if sub-optimal concentrations of romidepsin could be used in a combination treatment strategy, to either sensitize chondrosarcoma to non-epigenetic therapies or to reduce HDAC inhibitor toxicity. However, HDAC inhibition could not sensitize chondrosarcoma cells to four different types of chemotherapy (i.e., aclarubicin, cisplatin, doxorubicin, and temozolomide), although this has been extensively described in other tumor types [37]. Only the combinations of romidepsin with two metabolic compounds (i.e., chloroquine and metformin) and four Bcl-2 family member inhibitors (i.e., ABT-737, venetoclax, WEHI-539, and S63845) were synergistic in chondrosarcoma cell lines. HDAC inhibitors highly alter the metabolic state of glioblastoma cell lines [51], and a similar

mechanism in chondrosarcoma could underlie the sensitization to the glutaminolytic pathway inhibitors chloroquine and metformin. However, in breast cancer the synergistic effect between HDAC inhibition and chloroquine has been ascribed to the inhibition of the autophagic flux [52]. The synergistic effect between HDAC inhibition and Bcl-2 family member inhibitors in chondrosarcoma might be caused by an imbalance between pro- and anti-apoptotic Bcl-2 family members. We showed that romidepsin changes the expression levels of these proteins and shifts the balance to a more pro-apoptotic phenotype. Concomitant inhibition of anti-apoptotic Bcl-2 family members will further lower the apoptotic threshold, leading to a more pronounced induction of apoptosis as compared to single agent treatment. Changes in the expression of the pro- and anti-apoptotic Bcl-2 family members due to HDAC inhibition have been observed in several other tumor types [53–55]. The exact mechanism underlying the changes in the expression of these proteins is not completely understood, although one study ascribes it to local deacetylation of histone H3 at Bcl-2 promoters [53], suggesting that HDAC inhibitors could regulate the transcriptional activity of Bcl-2 family member genes. The biological mechanism underlying the synergistic effect between HDAC inhibition and glutaminolysis or Bcl-2 family member inhibition in chondrosarcoma warrants further investigation. Since several clinical trials have shown that solid tumors are resistant to HDAC inhibitor monotherapy [56], the identified combination therapies could help to increase the therapeutic potential of both HDAC inhibitors and the small molecule inhibitors in chondrosarcoma.

Conclusions

In summary, alterations in the methylome of *IDH* mutant cartilage tumors are associated with tumor progression and this study shows that targeting of epigenetic regulators could be a potential therapeutic strategy for both *IDH* wildtype and *IDH* mutant chondrosarcoma patients. Our study establishes that HDAC enzymes play a prominent role in the epigenetic landscape and survival of chondrosarcoma cells, especially class I HDACs. Chondrosarcoma cell lines are highly sensitive to the class I HDAC inhibitor romidepsin, irrespective of the chondrosarcoma subtype or the *IDH* mutation status. In addition, our study identifies glutaminolysis and Bcl-2 family member inhibitors as potential candidates to be used in combination with HDAC inhibition, suggesting that romidepsin influences the metabolic state and apoptotic threshold of chondrosarcoma cells. Further studies are needed to elucidate the exact mechanisms underlying HDAC inhibitor sensitivity in chondrosarcoma and to confirm romidepsin efficacy in an orthotopic chondrosarcoma mouse model. Taken together, pharmacological inhibition of HDAC enzymes may represent a promising targeted therapeutic strategy for chondrosarcoma patients. In spite of the fact that the mechanisms underlying HDAC inhibitor sensitivity are currently unknown, the identifica-

tion of novel treatment strategies for chondrosarcoma remains an important objective, especially for patients with unresectable or high-grade tumors.

Acknowledgements

The authors thank Brendy E.W.M. van den Akker and Pauline M. Wijers-Koster for technical assistance, Johnny Suijker for establishing the long-term AGI-5198 treated JJ012 cell line and preparing cases for the methylation array, André J. van Wijnen for his help with the data analysis of the previously performed RNA sequencing, and A.G. Jochemsen for the fruitful discussions. The authors are grateful to J.A. Block (Rush University Medical Centre, Chicago, IL, USA) for the JJ012 cell line, A. Llombart-Bosch (University of Valencia, Spain) for the CH2879 and CH3573 cell lines, J.A. Fletcher for the MCS170 cell line, and T. Ariizumi (Niigata University Graduate School of Medical and Dental Sciences, Japan) for the NDCS1 cell line.

Author contributions

Conceptualization, S.V., E.H.J.D., and J.V.M.G.B.; Data curation, S.V. and J.O.; Formal analysis, S.V., J.O., and P.J.F.; Funding acquisition, J.V.M.G.B.; Investigation, S.V., A.B.K, Z.B., I.P., and I.H.B.-d.B.; Methodology, S.V., Z.B., I.P., E.H.J.D., and J.V.M.G.B.; Project administration, S.V. and J.V.M.G.B.; Supervision, J.V.M.G.B.; Visualization, S.V., J.O., and P.J.F.; Writing—original draft, S.V. and J.V.M.G.B.; Writing—review and editing, S.V., A.B.K, Z.B., I.P., I.H.B.-d.B., J.O., P.J.F., E.H.J.D., and J.V.M.G.B. All authors have read and agreed to the published version of the manuscript.

Funding

This work was financially supported by the Dutch Cancer Society (UL2013-6103).

References

[1] Bovée JVMG, Bloem JL, Flanagan AM, Nielsen GP, Yoshida A. Central atypical cartilaginous tumour / chondrosarcoma, grade 1. In: WHO Classification of Tumours Editorial Board (ed) *WHO Classification of Tumours - Soft Tissue and Bone Tumours*. Lyon, France, IARC Press, 2020, pp. 370–372.

[2] Bovée JVMG, Bloem JL, Flanagan AM, Nielsen GP, Yoshida A. Central chondrosarcoma, grades 2 and 3. In: WHO Classification of Tumours Editorial Board (ed) *WHO Classification of Tumours - Soft Tissue and Bone Tumours*. Lyon, France, IARC Press, 2020, pp. 375–378.

[3] Evans HL, Ayala AG, Romsdahl MM. Prognostic factors in chondrosarcoma of bone. A clinicopathologic analysis with emphasis on histologic grading. *Cancer* 1977; 40(2):818–831.

[4] Gelderblom H, Hogendoorn PCW, Dijkstra SD, van Rijswijk CS, Krol AD, Taminiau AHM, et al. The Clinical Approach Towards Chondrosarcoma. *Oncologist* 2008; 13(3):320–329.

[5] Amary MF, Bacsi K, Maggiani F, Damato S, Halai D, Berisha F, et al. IDH1 and IDH2 mutations are frequent events in central chondrosarcoma and central and periosteal chondromas but not in other mesenchymal tumours. *J Pathol* 2011; 224(3):334–343.

[6] Pansuriya TC, Van Eijk R, D'Adamo P, Van Ruler MAJH, Kuijjer ML, Oosting J, et al. Somatic mosaic IDH1 and IDH2 mutations are associated with enchondroma and spindle cell hemangioma in Ollier disease and Maffucci syndrome. *Nat Genet* 2011; 43(12):1256–1261.

[7] Dang L, White DW, Gross S, Bennett BD, Bittinger MA, Driggers EM, et al. Cancer-associated IDH1 mutations produce 2-hydroxyglutarate. *Nature* 2009; 462(7274):739–744.

[8] Molenaar RJ, Radivoyevitch T, Maciejewski JP, van Noorden CJF, Bleeker FE. The driver and passenger effects of isocitrate dehydrogenase 1 and 2 mutations in oncogenesis and survival prolongation. *Biochim Biophys Acta* 2014; 1846(2):326–341.

[9] Pusch S, Schweizer L, Beck AC, Lehmler JM, Weissert S, Balss J, et al. D-2-Hydroxyglutarate producing neo-enzymatic activity inversely correlates with frequency of the type of isocitrate dehydrogenase 1 mutations found in glioma. *Acta Neuropathol Commun* 2014; 2:19.

[10] Xu W, Yang H, Liu Y, Yang Y, Wang P, Kim SH, et al. Oncometabolite 2-hydroxyglutarate is a competitive inhibitor of α-ketoglutarate-dependent dioxygenases. *Cancer Cell* 2011; 19(1):17–30.

[11] Chowdhury R, Yeoh KK, Tian YM, Hillringhaus L, Bagg EA, Rose NR, et al. The oncometabolite 2-hydroxyglutarate inhibits histone lysine demethylases. *EMBO Rep* 2011; 12(5):463–469.

[12] Reitman ZJ, Jin G, Karoly ED, Spasojevic I, Yang J, Kinzler KW, et al. Profiling the effects of isocitrate dehydrogenase 1 and 2 mutations on the cellular metabolome. *Proc Natl Acad Sci* 2011; 108(8):3270–3275.

[13] M. Gagné L, Boulay K, Topisirovic I, Huot MÉ, Mallette FA. Oncogenic Activities of IDH1/2 Mutations: From Epigenetics to Cellular Signaling. *Trends Cell Biol* 2017; 27(10):738–752.

[14] Hirata M, Sasaki M, Cairns RA, Inoue S, Puviindran V, Li WY, et al. Mutant IDH is sufficient to initiate enchondromatosis in mice. *Proc Natl Acad Sci* 2015; 112(9):2829–2834.

[15] Jin Y, Elalaf H, Watanabe M, Tamaki S, Hineno S, Matsunaga K, et al. Mutant idh1 dysregulates the differentiation of mesenchymal stem cells in association with gene-specific histone modifications to cartilage- and bone-related genes. *PLoS One* 2015; 10(7):e0131998.

[16] Suijker J, Baelde HJ, Roelofs H, Cleton-Jansen AM, Bovée JVMG. The oncometabolite D-2-hydroxyglutarate induced by mutant IDH1 or -2 blocks osteoblast differentiation in vitro and in vivo. *Oncotarget* 2015; 6(17):14832–14842.

[17] Guilhamon P, Eskandarpour M, Halai D, Wilson GA, Feber A, Teschendorff AE, et al. Meta-analysis of IDH-mutant cancers identifies EBF1 as an interaction partner for TET2. *Nat Commun* 2013; 4:2166.

[18] Suijker J, Oosting J, Koornneef A, Struys EA, Salomons GS, Schaap FG, et al. Inhibition of mutant IDH1 decreases D-2-HG levels without affecting tumorigenic properties of chondrosarcoma cell lines. *Oncotarget* 2015; 6(14):12505–12519.

[19] Goeman JJ, Van de Geer S, De Kort F, van Houwellingen HC. A global test for groups fo genes: Testing association with a clinical outcome. *Bioinformatics* 2004; 20(1):93–99.

[20] Teschendorff AE, Marabita F, Lechner M, Bartlett T, Tegner J, Gomez-Cabrero D, et al. A beta-mixture quantile normalization method for correcting probe design bias in Illumina Infinium 450 k DNA methylation data. *Bioinformatics* 2013; 29(2):189–196.

[21] Alhamdoosh M, Ng M, Wilson NJ, Sheridan JM, Huynh H, Wilson MJ, et al. Combining multiple tools outperforms individual methods in gene set enrichment analyses. *Bioinformatics* 2017; 33(3):414–424.

[22] Gil-Benso R, Lopez-Gines C, López-Guerrero JA, Carda C, Callaghan RC, Navarro S, et al. Establishment and characterization of a continuous human chondrosarcoma cell line, ch-2879: Comparative histologic and genetic studies with its tumor of origin. *Lab Investig* 2003; 83(6):877–887.

[23] Scully SP, Berend KR, Toth A, Qi WN, Qi Z, Block JA. Interstitial collagenase gene expression correlates with in vitro invasion in human chondrosarcoma. *Clin Orthop Relat Res* 2000; (376):291–303.

[24] Calabuig-Fariñas S, Benso RG, Szuhai K, Machado I, López-Guerrero JA, De Jong D, et al. Characterization of a new human cell line (CH-3573) derived from a grade II chondrosarcoma with matrix production. *Pathol Oncol Res* 2012; 18(4):793–802.

[25] van Oosterwijk JG, de Jong D, van Ruler MA, Hogendoorn PC, Dijkstra PS, van Rijswijk CS, et al. Three new chondrosarcoma cell lines: one grade III conventional central chondrosarcoma and two dedifferentiated chondrosarcomas of bone. *BMC Cancer* 2012; 12:375.

[26] Kudo N, Ogose A, Hotta T, Kawashima H, Gu W, Umezu H, et al. Establishment of novel human dedifferentiated chondrosarcoma cell line with osteoblastic differentiation. *Virchows Arch* 2007; 451(3):691–699.

[27] Rasheed S, Nelson-Rees WA, Toth EM, Arnstein P, Gardner MB. Characterization of a newly derived human sarcoma cell line (HT-1080). *Cancer* 1974; 33(4):1027–1033.

[28] De Jong Y, Van Maldegem AM, Marino-Enriquez A, De Jong D, Suijker J, Briaire-De Bruijn IH, et al. Inhibition of Bcl-2 family members sensitizes mesenchymal chondrosarcoma to conventional chemotherapy: Report on a novel mesenchymal chondrosarcoma cell line. *Lab Investig* 2016; 96(10):1128–1137.

[29] Venneker S, Kruisselbrink AB, Briaire-de Bruijn IH, de Jong Y, van Wijnen AJ, Danen EHJ, et al. Inhibition of PARP Sensitizes Chondrosarcoma Cell Lines to Chemo- and Radiotherapy Irrespective of the IDH1 or IDH2 Mutation Status. *Cancers (Basel)* 2019; 11(12):1918.

[30] Palubeckaitė I, Venneker S, Briaire-de Bruijn IH, van den Akker B, Krol AD, Gelderblom H, et al. Selection of effective therapies using three-dimensional in vitro modelling of chondrosarcoma. *Front Mol Biosci* 2020; 7:566291.

[31] Zhang JH, Chung TDY, Oldenburg KR. A simple statistical parameter for use in evaluation and validation of high throughput screening assays. *J Biomol Screen* 1999; 4(2):67–73.

[32] Greco W, Bravo G, Parsons J. The search for Synergy: A critical review from a repsonse persepective. *Pharmacol Rev* 1995; 47(2):331–385.

[33] Borisy AA, Elliott PJ, Hurst NW, Lee MS, Lehar J, Price ER, et al. Systematic discovery of multicomponent therapeutics. *Proc Natl Acad Sci* 2003; 100(13):7977–7982.

[34] Rohle D, Popovici-Muller J, Palaskas N, Turcan S, Grommes C, Campos C, et al. An inhibitor of mutant IDH1 delays growth and promotes differentiation of glioma cells. *Science* 2013; 340(6132):626–630.

[35] Furumai R, Matsuyama A, Kobashi N, Lee KH, Nishiyama M, Nakajima H, et al. FK228 (depsipeptide) as a natural prodrug that inhibits class I histone deacetylases. *Cancer Res* 2002; 62(17):4916–4921.

[36] Bradner JE, West N, Grachan ML, Greenberg EF, Haggarty SJ, Warnow T, et al. Chemical phylogenetics of histone deacetylases. *Nat Chem Biol* 2010; 6(3):238–243.

[37] Suraweera A, O'Byrne KJ, Richard DJ. Combination therapy with histone deacetylase inhibitors (HDACi) for the treatment of cancer: Achieving the full therapeutic potential of HDACi. *Frontiers in Oncology* 2018; 8:92.

[38] Peterse EFP, van den Akker BEWM, Niessen B, Oosting J, Suijker J, de Jong Y, et al. NAD Synthesis Pathway Interference Is a Viable Therapeutic Strategy for Chondrosarcoma. *Mol Cancer Res* 2017; 15(12):1714–1721.

[39] Chen C, Liu Y, Lu C, Cross JR, Morris IV JP, Shroff AS, et al. Cancer-associated IDH2 mutants drive an acute myeloid leukemia that is susceptible to Brd4 inhibition. *Genes Dev* 2013; 27(18):1974–1985.

[40] Turcan S, Fabius AW, Borodovsky A, Pedraza A, Brennan C, Huse J, et al. Efficient induction of differentiation and growth inhibition in IDH1 mutant glioma cells by the DNMT Inhibitor Decitabine. *Oncotarget* 2013; 4(10):1729–1736.

[41] Borodovsky A, Salmasi V, Turcan S, Fabius AWM, Baia G, Eberhart CG, et al. 5-azacytidine reduces methylation, promotes differentiation and induces tumor regression in a patient-derived IDH1 mutant glioma xenograft. *Oncotarget* 2013; 4(10):1737–1747.

[42] de Jong Y, Bennani F, van Oosterwijk JG, Alberti G, Baranski Z, Wijers-Koster P, et al. A screening-based approach identifies cell cycle regulators AURKA, CHK1 and PLK1 as targetable regulators of chondrosarcoma cell survival. *J Bone Oncol* 2019; 19:100268.

[43] Bradley EW, Carpio LR, van Wijnen AJ, McGee-Lawrence ME, Westendorf JJ. Histone Deacetylases in Bone Development and Skeletal Disorders. *Physiol Rev* 2015; 95(4):1359–1381.

[44] Hong S, Derfoul A, Pereira-Mouries L, Hall DJ. A novel domain in histone deacetylase 1 and 2 mediates repression of cartilage-specific genes in human chondrocytes. *FASEB J* 2009; 23(10):3539–3552.

[45] Sakimura R, Tanaka K, Yamamoto S, Matsunobu T, Li X, Hanada M, et al. The effects of histone deacetylase inhibitors on the induction of differentiation in chondrosarcoma cells. *Clin Cancer Res* 2007; 13(1):275–282.

[46] Zhu J, Gu J, Ma J, Xu Z, Tao H. Histone deacetylase inhibitors repress chondrosarcoma cell proliferation. *J BUON* 2015; 20(1):269–274.

[47] Piekarz RL, Robey RW, Zhan Z, Kayastha G, Sayah A, Abdeldaim AH, et al. T-cell lymphoma as a model for the use of histone deacetylase inhibitors in cancer therapy: Impact of depsipeptide on molecular markers, therapeutic targets, and mechanisms of resistance. *Blood* 2004; 103(12):4636–4643.

[48] Valdez BC, Brammer JE, Li Y, Murray D, Liu Y, Hosing C, et al. Romidepsin targets multiple survival signaling pathways in malignant T cells. *Blood Cancer J* 2015; 5(10):e357.

[49] Woo S, Gardner ER, Chen X, Ockers SB, Baum CE, Sissung TM, et al. Population pharmacokinetics of romidepsin in patients with cutaneous T-cell lymphoma and relapsed peripheral T-cell lymphoma. *Clin Cancer Res* 2009; 15(4):1496–1503.

[50] van Oosterwijk JG, Plass JRM, Meijer D, Que I, Karperien M, Bovée JVMG. An orthotopic mouse model for chondrosarcoma of bone provides an in vivo tool for drug testing. *Virchows Arch* 2015; 466(1):101–109.

[51] Cuperlovic-Culf M, Touaibia M, St-Coeur PD, Poitras J, Morin P, Culf AS. Metabolic effects of known and novel HDAC and SIRT inhibitors in glioblastomas independently or combined with temozolomide. *Metabolites* 2014; 4(3):807–830.

[52] Rao R, Balusu R, Fiskus W, Mudunuru U, Venkannagari S, Chauhan L, et al. Combination of pan-histone deacetylase inhibitor and autophagy inhibitor exerts superior efficacy against triple-negative human breast cancer cells. *Mol Cancer Ther* 2012; 11(4):973–983.

[53] Duan H, Heckman CA, Boxer LM. Histone Deacetylase Inhibitors Down-Regulate bcl-2 Expression and Induce Apoptosis in t(14;18) Lymphomas. *Mol Cell Biol* 2005; 25(5):1608–1619.

[54] Zhang XD, Gillespie SK, Borrow JM, Hersey P. The histone deacetylase inhibitor suberic bishydroxamate regulates the expression of multiple apoptotic mediators and induces mitochondria-dependent apoptosis of melanoma cells. *Mol Cancer Ther* 2004; 3(4):425–435.

[55] Bolden JE, Shi W, Jankowski K, Kan CY, Cluse L, Martin BP, et al. HDAC inhibitors induce tumor-cell-selective pro-apoptotic transcriptional responses. *Cell Death Dis* 2013; 4(2):e519.

[56] Slingerland M, Guchelaar HJ, Gelderblom H. Histone deacetylase inhibitors: An overview of the clinical studies in solid tumors. *Anticancer Drugs* 2014; 25(2):140–149.

Supplementary tables

Table S1. Characteristics of patient samples that were used for the DNA methylation array.

Sample ID	Tumor Location	Tumor Type	Grade	*IDH1* Mutation	*IDH2* Mutation	CIMP-Status
L19	Femur	CS	II	-	R172S	Positive
L186	Scapula	CS	II	R132C	-	Positive
L205	Humerus	EC	-	-	R172M	Positive
L223	Tibia	CS	II	R132C	-	Positive
L314	Radius	CS	ACT/I	R132H	-	Positive
L533	Humerus	CS	ACT/I	R132S	-	Negative
L646	Unknown	CS	II	R132C	-	Positive
L738	Unknown	CS	ACT/I	R132S	-	Positive
L855	Digit	CS	II	R132G	-	Positive
L869	Tibia	CS	II	R132C	-	Positive
L1326	Axilla	CS	III	R132C	-	Positive
L1491	Ulna	EC	-	R132H	-	Positive
L1536	Unknown	CS	II	R132G	-	Positive
L1539	Femur	CS	ACT/I	R132L	-	Positive
L1769	Femur	CS	ACT/I	R132H	-	Negative
L1829	Tibia	EC	-	R132C	-	Positive
L1993	Unknown	CS	III	R132C	-	Positive
L2088	Femur	CS	III	R132C	-	Positive
L2814	Femur	CS	II	R132C	-	Positive
L3529	Femur	CS	ACT/I	R132S	-	Positive

EC: enchondroma, ACT: atypical cartilaginous tumor, CS: chondrosarcoma.

Table S2. Significantly differentially methylated genes in benign/low-grade and high-grade cartilage tumors.

Strongly Methylated in Benign/Low-Grade Tumors (*n* = 89)		
Gene	***p*-Value**	**Difference in β-Value**
ZFAND2A	1.82×10^{-6}	-0.074
DUSP14	3.37×10^{-6}	-0.105
TNFRSF25	1.05×10^{-5}	-0.334
TCEA2	1.82×10^{-5}	-0.068
DIXDC1	2.12×10^{-5}	-0.067
PHC3	3.68×10^{-5}	-0.053
DUS1L	5.77×10^{-5}	-0.086
MT2A	6.62×10^{-5}	-0.135
C9orf69	6.98×10^{-5}	-0.038
VPS13D	7.60×10^{-5}	-0.045
VEGFA	7.90×10^{-5}	-0.096
MRPL11	9.18×10^{-5}	-0.050
SERPINH1	1.00×10^{-4}	-0.052
C3orf21	1.05×10^{-4}	-0.046
RER1	1.31×10^{-4}	-0.066
MORN1	1.31×10^{-4}	-0.066
B4GALT4	1.39×10^{-4}	-0.019
KCTD11	1.42×10^{-4}	-0.060
C5orf27	1.43×10^{-4}	-0.065
ZMYND8	2.14×10^{-4}	-0.061
WHAMM	2.41×10^{-4}	-0.061
C14orf79	2.44×10^{-4}	-0.016
STK3	2.75×10^{-4}	-0.052
TRIM4	2.91×10^{-4}	-0.035
C18orf45	2.95×10^{-4}	-0.080
FRMD4A	2.99×10^{-4}	-0.213
RNU6ATAC	3.63×10^{-4}	-0.063
RIN1	3.72×10^{-4}	-0.082
KLHL21	3.78×10^{-4}	-0.044
PNPLA2	3.84×10^{-4}	-0.017
C19orf61	5.11×10^{-4}	-0.033
PSMD9	5.45×10^{-4}	-0.024
ARFGAP1	5.51×10^{-4}	-0.021
TMEM121	6.04×10^{-4}	-0.067
KAZALD1	6.76×10^{-4}	-0.041
MINPP1	8.02×10^{-4}	-0.060
TRAF4	8.87×10^{-4}	-0.004
SNRPD1	9.02×10^{-4}	-0.031

Table S2. Significantly differentially methylated genes in benign/low-grade and high-grade cartilage tumors. (*continued*)

Strongly Methylated in Benign/Low-Grade Tumors (*n* = 89)		
Gene	***p*-Value**	**Difference in β-Value**
GADD45B	9.68×10^{-4}	-0.031
DNAJB13	1.00×10^{-3}	-0.381
SPATA6	1.00×10^{-3}	-0.018
RBM28	1.09×10^{-3}	-0.010
EXOG	1.11×10^{-3}	-0.049
SOCS3	1.11×10^{-3}	-0.111
ORAOV1	1.21×10^{-3}	-0.021
HLCS	1.21×10^{-3}	-0.039
ATP8B4	1.22×10^{-3}	-0.290
GAPDH	1.29×10^{-3}	-0.025
GINS4	1.34×10^{-3}	-0.031
PPM1G	1.35×10^{-3}	-0.039
PLCL2	1.40×10^{-3}	-0.218
SNX21	1.42×10^{-3}	-0.022
GPS2	1.42×10^{-3}	-0.062
ANKRD46	1.45×10^{-3}	-0.016
CCNH	1.47×10^{-3}	-0.016
PATL1	1.69×10^{-3}	-0.034
C3orf67	1.72×10^{-3}	-0.031
ITCH	1.75×10^{-3}	-0.020
ASXL2	1.80×10^{-3}	-0.001
PHKG2	1.87×10^{-3}	-0.017
GARS	1.91×10^{-3}	-0.034
MIR548H4	1.95×10^{-3}	-0.021
GLCE	1.95×10^{-3}	-0.021
ADRM1	1.97×10^{-3}	-0.047
BPHL	2.01×10^{-3}	-0.024
DKFZP686I15217	2.14×10^{-3}	-0.005
AGFG1	2.19×10^{-3}	-0.063
FAM188A	2.21×10^{-3}	-0.044
DUSP19	2.22×10^{-3}	-0.008
OGG1	2.24×10^{-3}	-0.025
BBS2	2.26×10^{-3}	-0.021
USP22	2.26×10^{-3}	-0.011
TM2D3	2.27×10^{-3}	-0.061
DCTN4	2.28×10^{-3}	-0.041
ABHD14B	2.33×10^{-3}	-0.018

Table S2. Significantly differentially methylated genes in benign/low-grade and high-grade cartilage tumors. (*continued*)

Strongly Methylated in Benign/Low-Grade Tumors (*n* = 89)		
Gene	***p*-Value**	**Difference in β-Value**
ABHD14A	2.33×10^{-3}	-0.018
RPL27A	2.42×10^{-3}	-0.009
TSSK6	2.50×10^{-3}	-0.071
NDUFA13	2.50×10^{-3}	-0.071
SENP5	2.58×10^{-3}	-0.013
MAMSTR	2.71×10^{-3}	-0.121
FAM91A1	2.80×10^{-3}	-0.018
PPP2CB	2.94×10^{-3}	-0.076
FNDC8	3.11×10^{-3}	-0.164
ZNF34	3.14×10^{-3}	-0.039
ZFP36	3.26×10^{-3}	-0.022
SLC22A15	3.41×10^{-3}	-0.215
CENPH	3.41×10^{-3}	-0.040
DGCR6	3.47×10^{-3}	-0.041

Table S2. Significantly differentially methylated genes in benign/low-grade and high-grade cartilage tumors. *(continued)*

Strongly Methylated in High-Grade Tumors (*n* = 592)		
Gene	***p*-Value**	**Difference in β-Value**
CEBPA	1.64×10^{-12}	0.311
LBX2	1.80×10^{-10}	0.488
SLC17A9	4.60×10^{-9}	0.455
C9orf167	6.79×10^{-9}	0.459
KCTD1	7.01×10^{-9}	0.159
CDCA7L	2.17×10^{-8}	0.367
SPRED3	2.27×10^{-8}	0.360
PROCA1	2.33×10^{-8}	0.319
AP1S3	2.93×10^{-8}	0.135
NRBP1	3.09×10^{-8}	0.054
RNF122	7.08×10^{-8}	0.057
CDKN2BAS	9.92×10^{-8}	0.087
ITGB7	1.02×10^{-7}	0.274
CHD5	1.26×10^{-7}	0.308
REC8	1.85×10^{-7}	0.273
ATG9B	2.27×10^{-7}	0.208
NOS3	2.27×10^{-7}	0.208
PDE4C	2.41×10^{-7}	0.138
NCRNA00085	2.69×10^{-7}	0.385
ZNF771	3.15×10^{-7}	0.161
P2RY1	3.92×10^{-7}	0.336
PTGER4	4.24×10^{-7}	0.356
MAL	5.20×10^{-7}	0.140
STX1B	6.11×10^{-7}	0.215
CRIP1	7.05×10^{-7}	0.333
EMILIN2	7.39×10^{-7}	0.181
SARM1	7.62×10^{-7}	0.191
PIK3AP1	8.33×10^{-7}	0.118
ARNTL2	8.69×10^{-7}	0.108
SYNGR3	8.97×10^{-7}	0.332
SEL1L3	1.29×10^{-6}	0.275
FOXP4	1.44×10^{-6}	0.271
NFATC2	1.49×10^{-6}	0.221
FUZ	1.59×10^{-6}	0.121
CYBA	1.62×10^{-6}	0.447
RINL	1.65×10^{-6}	0.244
PCDHGC5	1.74×10^{-6}	0.271

Table S2. Significantly differentially methylated genes in benign/low-grade and high-grade cartilage tumors. (*continued*)

Strongly Methylated in High-Grade Tumors (*n* = 592)		
Gene	***p*-Value**	**Difference in β-Value**
PCDHGC4	1.74×10^{-6}	0.271
CACNA1C	1.75×10^{-6}	0.319
ADAM8	1.81×10^{-6}	0.391
VSIG10L	1.97×10^{-6}	0.153
BZRAP1	2.06×10^{-6}	0.234
IGF1R	2.07×10^{-6}	0.188
GMPPA	2.13×10^{-6}	0.073
TBC1D10C	2.22×10^{-6}	0.130
C8orf73	2.43×10^{-6}	0.341
ABCC1	2.47×10^{-6}	0.043
ACP5	2.51×10^{-6}	0.229
HRAS	2.56×10^{-6}	0.166
B4GALT6	3.13×10^{-6}	0.183
TRAF5	3.22×10^{-6}	0.093
AFF1	3.45×10^{-6}	0.073
EPC1	3.52×10^{-6}	0.129
MGA	3.69×10^{-6}	0.279
SH2D3A	4.24×10^{-6}	0.258
RREB1	4.41×10^{-6}	0.128
HIST1H3J	4.70×10^{-6}	0.446
ICAM5	5.09×10^{-6}	0.369
PCDHGA4	5.17×10^{-6}	0.083
PCDHGA12	5.17×10^{-6}	0.083
PCDHGA11	5.17×10^{-6}	0.083
PCDHGA9	5.17×10^{-6}	0.083
PCDHGA1	5.17×10^{-6}	0.083
PCDHGB1	5.17×10^{-6}	0.083
PCDHGC3	5.17×10^{-6}	0.083
PCDHGB6	5.17×10^{-6}	0.083
PCDHGB3	5.17×10^{-6}	0.083
PCDHGB7	5.17×10^{-6}	0.083
PCDHGA6	5.17×10^{-6}	0.083
PCDHGA8	5.17×10^{-6}	0.083
PCDHGA10	5.17×10^{-6}	0.083
PCDHGA5	5.17×10^{-6}	0.083
PCDHGB4	5.17×10^{-6}	0.083
PCDHGA3	5.17×10^{-6}	0.083

Table S2. Significantly differentially methylated genes in benign/low-grade and high-grade cartilage tumors. (*continued*)

Strongly Methylated in High-Grade Tumors (*n* = 592)		
Gene	***p*-Value**	**Difference in β-Value**
PCDHGA2	5.17×10^{-6}	0.083
PCDHGA7	5.17×10^{-6}	0.083
PCDHGB2	5.17×10^{-6}	0.083
PCDHGB5	5.17×10^{-6}	0.083
ENC1	5.43×10^{-6}	0.162
ST6GAL1	5.82×10^{-6}	0.241
ALDH5A1	6.08×10^{-6}	0.182
PHF11	6.09×10^{-6}	0.201
ITPKA	6.13×10^{-6}	0.425
STAT4	6.42×10^{-6}	0.319
IFI30	6.45×10^{-6}	0.163
ADRBK1	6.48×10^{-6}	0.134
DMC1	6.71×10^{-6}	0.264
HIST1H4D	7.68×10^{-6}	0.273
ADORA2A	8.84×10^{-6}	0.161
ABI3	9.09×10^{-6}	0.526
GNGT2	9.09×10^{-6}	0.526
DHH	9.11×10^{-6}	0.349
DNAH3	9.27×10^{-6}	0.139
TMEM159	9.27×10^{-6}	0.139
FAM110A	9.74×10^{-6}	0.156
LMTK3	1.10×10^{-5}	0.111
IL23A	1.16×10^{-5}	0.256
CORO6	1.19×10^{-5}	0.203
LFNG	1.19×10^{-5}	0.102
TBC1D1	1.25×10^{-5}	0.072
TNFRSF1B	1.36×10^{-5}	0.192
TYMP	1.47×10^{-5}	0.153
LIMD2	1.48×10^{-5}	0.132
IKZF3	1.52×10^{-5}	0.221
ZNF808	1.56×10^{-5}	0.514
C17orf46	1.56×10^{-5}	0.355
NTNG2	1.57×10^{-5}	0.161
IL15RA	1.62×10^{-5}	0.126
SLCO5A1	1.63×10^{-5}	0.175
CD74	1.64×10^{-5}	0.263
KIAA1522	1.71×10^{-5}	0.106

Table S2. Significantly differentially methylated genes in benign/low-grade and high-grade cartilage tumors. (*continued*)

Strongly Methylated in High-Grade Tumors (*n* = 592)		
Gene	***p*-Value**	**Difference in β-Value**
MGC29506	1.81×10^{-5}	0.129
CACNA2D2	1.92×10^{-5}	0.290
S1PR4	2.06×10^{-5}	0.150
KIAA0562	2.11×10^{-5}	0.063
DFFB	2.23×10^{-5}	0.059
FGR	2.27×10^{-5}	0.161
GOLM1	2.28×10^{-5}	0.354
TM7SF2	2.28×10^{-5}	0.331
FCHO1	2.32×10^{-5}	0.148
WNT1	2.35×10^{-5}	0.269
BATF3	2.37×10^{-5}	0.145
MKNK2	2.40×10^{-5}	0.213
RRBP1	2.43×10^{-5}	0.047
KIAA1274	2.44×10^{-5}	0.126
NHLRC4	2.47×10^{-5}	0.081
FAM107B	2.47×10^{-5}	0.171
HTATIP2	2.49×10^{-5}	0.323
CYTH2	2.54×10^{-5}	0.095
HHEX	2.56×10^{-5}	0.119
LIPE	2.71×10^{-5}	0.228
INPP5D	2.73×10^{-5}	0.154
LRRC8C	2.89×10^{-5}	0.063
LOC606724	2.89×10^{-5}	0.116
RAB24	2.99×10^{-5}	0.038
GADD45G	3.00×10^{-5}	0.302
C9orf66	3.00×10^{-5}	0.268
DOCK8	3.00×10^{-5}	0.268
ZBTB44	3.08×10^{-5}	0.049
OSM	3.08×10^{-5}	0.132
PRR5L	3.16×10^{-5}	0.105
C8orf51	3.18×10^{-5}	0.077
RHPN1	3.18×10^{-5}	0.077
ZNF296	3.43×10^{-5}	0.281
KRTCAP3	3.43×10^{-5}	0.289
FAM78A	3.74×10^{-5}	0.222
SLC9A3R1	3.82×10^{-5}	0.111
SERPINB9	3.90×10^{-5}	0.325

Table S2. Significantly differentially methylated genes in benign/low-grade and high-grade cartilage tumors. (*continued*)

Strongly Methylated in High-Grade Tumors (*n* = 592)		
Gene	***p*-Value**	**Difference in β-Value**
HMHA1	4.02×10^{-5}	0.134
DNMT3A	4.04×10^{-5}	0.146
CARHSP1	4.41×10^{-5}	0.048
SLC29A2	4.43×10^{-5}	0.089
CFLAR	4.58×10^{-5}	0.227
GDI2	4.63×10^{-5}	0.029
HDAC3	4.78×10^{-5}	0.115
RELL2	4.78×10^{-5}	0.115
FRAT1	4.79×10^{-5}	0.071
IER3	5.54×10^{-5}	0.258
QRFP	5.64×10^{-5}	0.117
ONECUT1	5.66×10^{-5}	0.237
PYCARD	5.70×10^{-5}	0.264
SH2B3	5.70×10^{-5}	0.110
LPAR2	5.79×10^{-5}	0.329
TK2	5.88×10^{-5}	0.062
C1orf38	6.05×10^{-5}	0.120
LRRC20	6.05×10^{-5}	0.089
ATP2B4	6.18×10^{-5}	0.139
LOC146880	6.20×10^{-5}	0.380
BMP8B	6.39×10^{-5}	0.179
ABCA7	6.55×10^{-5}	0.097
LOC100133991	6.70×10^{-5}	0.199
CDKN2A	6.72×10^{-5}	0.125
FERMT3	6.90×10^{-5}	0.136
RAB3D	6.92×10^{-5}	0.327
CCDC88B	7.08×10^{-5}	0.048
C17orf62	7.28×10^{-5}	0.094
LTB4R2	7.46×10^{-5}	0.211
LTB4R	7.46×10^{-5}	0.211
CIDEB	7.46×10^{-5}	0.211
PTEN	7.50×10^{-5}	0.333
KILLIN	7.50×10^{-5}	0.333
EPHA4	7.54×10^{-5}	0.079
UBE2Q2	7.67×10^{-5}	0.261
SNN	7.67×10^{-5}	0.065
HCST	8.21×10^{-5}	0.382

Table S2. Significantly differentially methylated genes in benign/low-grade and high-grade cartilage tumors. (*continued*)

Strongly Methylated in High-Grade Tumors (*n* = 592)		
Gene	***p*-Value**	**Difference in β-Value**
UNKL	8.51×10^{-5}	0.088
ABCG1	8.57×10^{-5}	0.145
NTN1	8.59×10^{-5}	0.334
CHST12	8.74×10^{-5}	0.058
NRGN	8.87×10^{-5}	0.339
ANKRD23	9.15×10^{-5}	0.265
MFNG	9.17×10^{-5}	0.126
PRAGMIN	9.38×10^{-5}	0.238
CYP2U1	9.53×10^{-5}	0.098
HMGA1	9.80×10^{-5}	0.097
MYD88	9.84×10^{-5}	0.285
FAM102B	9.84×10^{-5}	0.112
BTBD11	9.88×10^{-5}	0.123
EMP3	1.01×10^{-4}	0.162
TNFRSF10A	1.05×10^{-4}	0.219
ANKRD28	1.11×10^{-4}	0.105
STK38	1.13×10^{-4}	0.025
MAP4K1	1.17×10^{-4}	0.073
EIF3K	1.17×10^{-4}	0.073
SNED1	1.17×10^{-4}	0.095
ISL2	1.17×10^{-4}	0.236
ALOX5AP	1.21×10^{-4}	0.175
MST1R	1.22×10^{-4}	0.125
HSBP1L1	1.24×10^{-4}	0.145
NUP210	1.29×10^{-4}	0.105
SNX32	1.30×10^{-4}	0.056
ACAA1	1.31×10^{-4}	0.228
CDC42BPG	1.32×10^{-4}	0.075
PIK3CD	1.33×10^{-4}	0.141
IL16	1.35×10^{-4}	0.058
RLTPR	1.39×10^{-4}	0.153
KCNAB2	1.40×10^{-4}	0.119
ETS2	1.43×10^{-4}	0.107
C9orf78	1.44×10^{-4}	0.081
USP20	1.44×10^{-4}	0.081
ANKRD34A	1.45×10^{-4}	0.028
RAB19	1.48×10^{-4}	0.330

Table S2. Significantly differentially methylated genes in benign/low-grade and high-grade cartilage tumors. (*continued*)

Strongly Methylated in High-Grade Tumors (*n* = 592)		
Gene	***p*-Value**	**Difference in β-Value**
KCNQ4	1.49×10^{-4}	0.329
SYNJ2	1.54×10^{-4}	0.060
DISP2	1.65×10^{-4}	0.057
GYG1	1.67×10^{-4}	0.017
ACP1	1.68×10^{-4}	0.058
SH3YL1	1.68×10^{-4}	0.058
LRRC37A3	1.77×10^{-4}	0.120
ALOX5	1.78×10^{-4}	0.236
B3GNT2	1.79×10^{-4}	0.175
GPR160	1.80×10^{-4}	0.060
TRAF1	1.81×10^{-4}	0.431
LYL1	1.82×10^{-4}	0.285
C14orf169	1.85×10^{-4}	0.190
HEATR4	1.85×10^{-4}	0.190
ADAMTSL5	1.87×10^{-4}	0.362
TRAPPC5	1.88×10^{-4}	0.083
RNF187	1.95×10^{-4}	0.046
ANKLE1	1.95×10^{-4}	0.240
NT5C3	1.95×10^{-4}	0.025
KLHDC5	1.96×10^{-4}	0.109
TP53TG5	2.00×10^{-4}	0.489
GJD3	2.10×10^{-4}	0.118
COTL1	2.13×10^{-4}	0.030
AXIN1	2.22×10^{-4}	0.057
HCG4P6	2.28×10^{-4}	0.299
ICAM1	2.30×10^{-4}	0.218
ZFAND2B	2.32×10^{-4}	0.024
PRKAG2	2.35×10^{-4}	0.101
FABP5	2.38×10^{-4}	0.302
EML5	2.38×10^{-4}	0.162
IL4I1	2.46×10^{-4}	0.065
NFIL3	2.47×10^{-4}	0.103
TMC4	2.53×10^{-4}	0.144
YPEL1	2.54×10^{-4}	0.062
LRPAP1	2.59×10^{-4}	0.061
EFCAB4B	2.60×10^{-4}	0.202
SLFN13	2.60×10^{-4}	0.275

Table S2. Significantly differentially methylated genes in benign/low-grade and high-grade cartilage tumors. (*continued*)

Strongly Methylated in High-Grade Tumors (*n* = 592)		
Gene	***p*-Value**	**Difference in β-Value**
NAGK	2.60×10^{-4}	0.042
GPR68	2.64×10^{-4}	0.141
RASSF2	2.67×10^{-4}	0.146
MTA2	2.67×10^{-4}	0.077
THSD1P	2.68×10^{-4}	0.131
CBX4	2.75×10^{-4}	0.042
RAB11FIP4	2.79×10^{-4}	0.234
TOX	2.79×10^{-4}	0.159
TTBK1	2.80×10^{-4}	0.209
MAPRE2	2.81×10^{-4}	0.161
LOC220930	2.85×10^{-4}	0.030
POU6F1	2.86×10^{-4}	0.032
C16orf54	2.87×10^{-4}	0.144
LYPD3	2.89×10^{-4}	0.274
CLSTN3	2.94×10^{-4}	0.398
CASP6	2.97×10^{-4}	0.021
MGAT1	2.98×10^{-4}	0.059
USP34	2.99×10^{-4}	0.079
MFSD2A	3.00×10^{-4}	0.294
EPSTI1	3.01×10^{-4}	0.290
SLC2A9	3.02×10^{-4}	0.157
IQGAP2	3.03×10^{-4}	0.163
TXNRD1	3.04×10^{-4}	0.200
DDX39	3.06×10^{-4}	0.274
CSK	3.06×10^{-4}	0.051
GMEB1	3.08×10^{-4}	0.055
ADD1	3.08×10^{-4}	0.047
FLI1	3.09×10^{-4}	0.170
ZMYM2	3.22×10^{-4}	0.086
RAB37	3.22×10^{-4}	0.236
PARP12	3.26×10^{-4}	0.125
PGS1	3.26×10^{-4}	0.066
ZC3HAV1	3.31×10^{-4}	0.056
ADCY4	3.32×10^{-4}	0.216
PPP1R15A	3.34×10^{-4}	0.036
ZFP90	3.37×10^{-4}	0.082
PRSS27	3.45×10^{-4}	0.165

Table S2. Significantly differentially methylated genes in benign/low-grade and high-grade cartilage tumors. (*continued*)

Strongly Methylated in High-Grade Tumors (*n* = 592)		
Gene	***p*-Value**	**Difference in β-Value**
TEC	3.50×10^{-4}	0.155
NMNAT3	3.51×10^{-4}	0.202
MEST	3.53×10^{-4}	0.103
HERC5	3.57×10^{-4}	0.070
CORO1A	3.61×10^{-4}	0.052
AMZ1	3.62×10^{-4}	0.248
RGS16	3.70×10^{-4}	0.261
VAV1	3.70×10^{-4}	0.171
LDLRAD2	3.73×10^{-4}	0.151
RNF44	3.80×10^{-4}	0.036
ZNF254	3.88×10^{-4}	0.470
FAM55C	3.89×10^{-4}	0.152
CD38	3.95×10^{-4}	0.140
CCDC61	4.02×10^{-4}	0.049
EML3	4.06×10^{-4}	0.053
CLIP2	4.07×10^{-4}	0.021
DSCR9	4.10×10^{-4}	0.151
HIST3H2BB	4.16×10^{-4}	0.296
C21orf122	4.20×10^{-4}	0.023
HLA-L	4.21×10^{-4}	0.085
FLYWCH2	4.31×10^{-4}	0.025
PTGER2	4.32×10^{-4}	0.303
SUSD1	4.37×10^{-4}	0.170
KLHDC7B	4.41×10^{-4}	0.180
SEMA7A	4.48×10^{-4}	0.187
FLOT1	4.52×10^{-4}	0.101
ZFPM1	4.61×10^{-4}	0.347
LOC651250	4.67×10^{-4}	0.161
ZEB1	4.74×10^{-4}	0.025
HPCAL1	4.75×10^{-4}	0.090
PTPRCAP	4.81×10^{-4}	0.092
QPCT	4.83×10^{-4}	0.279
RIPK3	4.87×10^{-4}	0.209
TRAPPC9	4.97×10^{-4}	0.056
SHF	4.97×10^{-4}	0.145
SFMBT1	4.99×10^{-4}	0.231
LOC100130557	4.99×10^{-4}	0.056

Table S2. Significantly differentially methylated genes in benign/low-grade and high-grade cartilage tumors. (*continued*)

Strongly Methylated in High-Grade Tumors (*n* = 592)		
Gene	***p*-Value**	**Difference in β-Value**
NUP153	5.03×10^{-4}	0.030
CCNI2	5.05×10^{-4}	0.123
TRIM59	5.15×10^{-4}	0.061
RBP5	5.17×10^{-4}	0.344
WIPF1	5.28×10^{-4}	0.049
BAMBI	5.43×10^{-4}	0.117
LINGO3	5.51×10^{-4}	0.414
DGAT2	5.54×10^{-4}	0.114
KCNIP2	5.55×10^{-4}	0.270
PAOX	5.56×10^{-4}	0.105
TMEM154	5.58×10^{-4}	0.101
LGALS9	5.58×10^{-4}	0.338
SIPA1	5.62×10^{-4}	0.222
CD72	5.64×10^{-4}	0.247
ZDHHC24	5.72×10^{-4}	0.136
ZEB2	5.95×10^{-4}	0.401
SNORA16A	5.97×10^{-4}	0.056
SNHG12	5.97×10^{-4}	0.056
POU3F2	5.98×10^{-4}	0.041
PATZ1	6.13×10^{-4}	0.100
HIST3H2A	6.15×10^{-4}	0.244
C11orf91	6.20×10^{-4}	0.143
CENPV	6.28×10^{-4}	0.141
CBY3	6.32×10^{-4}	0.094
GRK5	6.33×10^{-4}	0.041
TSPAN14	6.43×10^{-4}	0.029
MARCH3	6.52×10^{-4}	0.050
RASL11B	6.54×10^{-4}	0.162
CAMK1D	6.64×10^{-4}	0.113
TPM1	6.64×10^{-4}	0.227
CDKL2	6.78×10^{-4}	0.263
SNORD65	6.96×10^{-4}	0.112
MCF2L2	7.02×10^{-4}	0.080
BCAT1	7.26×10^{-4}	0.122
sep-01	7.49×10^{-4}	0.042
FLOT2	7.69×10^{-4}	0.030
TNPO2	7.69×10^{-4}	0.108

Table S2. Significantly differentially methylated genes in benign/low-grade and high-grade cartilage tumors. (*continued*)

Strongly Methylated in High-Grade Tumors (*n* = 592)		
Gene	***p*-Value**	**Difference in β-Value**
C5orf39	7.74×10^{-4}	0.304
RFC4	7.78×10^{-4}	0.009
MTRF1	8.00×10^{-4}	0.012
SPPL3	8.05×10^{-4}	0.065
PKN1	8.05×10^{-4}	0.054
ACTN3	8.10×10^{-4}	0.117
C9orf98	8.19×10^{-4}	0.132
NKX3-1	8.21×10^{-4}	0.106
CUL9	8.33×10^{-4}	0.082
NAGLU	8.49×10^{-4}	0.034
ANKRD53	8.51×10^{-4}	0.188
HEATR6	8.62×10^{-4}	0.055
ITGB2	8.72×10^{-4}	0.072
RPP25	8.82×10^{-4}	0.148
ADARB1	8.92×10^{-4}	0.018
TUBG2	8.97×10^{-4}	0.033
ZWILCH	9.01×10^{-4}	0.030
RPL4	9.01×10^{-4}	0.030
HLA-E	9.05×10^{-4}	0.064
PHLDA1	9.12×10^{-4}	0.206
SLC39A14	9.23×10^{-4}	0.077
ICAM3	9.25×10^{-4}	0.091
HPSE2	9.27×10^{-4}	0.092
SYNPO	9.28×10^{-4}	0.387
LY75	9.33×10^{-4}	0.218
KDM2B	9.33×10^{-4}	0.116
POMP	9.33×10^{-4}	0.029
ATP2A3	9.35×10^{-4}	0.099
BIRC3	9.41×10^{-4}	0.335
SORBS3	9.42×10^{-4}	0.237
RGS3	9.49×10^{-4}	0.155
WDR8	9.68×10^{-4}	0.059
CMC1	9.88×10^{-4}	0.020
KLF13	9.93×10^{-4}	0.106
C18orf1	1.00×10^{-3}	0.286
CTSZ	1.01×10^{-3}	0.047
FBXL22	1.06×10^{-3}	0.036

Table S2. Significantly differentially methylated genes in benign/low-grade and high-grade cartilage tumors. (*continued*)

Strongly Methylated in High-Grade Tumors (*n* = 592)		
Gene	***p*-Value**	**Difference in β-Value**
CCDC48	1.06×10^{-3}	0.245
PLAUR	1.10×10^{-3}	0.106
ATP11B	1.10×10^{-3}	0.063
ZC3HAV1L	1.11×10^{-3}	0.177
C19orf76	1.13×10^{-3}	0.259
BCL2	1.13×10^{-3}	0.140
VOPP1	1.14×10^{-3}	0.096
GPR3	1.16×10^{-3}	0.102
DNAH10	1.16×10^{-3}	0.347
MAP7D1	1.17×10^{-3}	0.069
TRIM2	1.18×10^{-3}	0.165
C14orf43	1.19×10^{-3}	0.025
UNC84B	1.19×10^{-3}	0.057
C1orf88	1.19×10^{-3}	0.102
SGEF	1.21×10^{-3}	0.120
AGMAT	1.21×10^{-3}	0.160
CD55	1.21×10^{-3}	0.064
C10orf18	1.23×10^{-3}	0.093
SGK1	1.26×10^{-3}	0.142
SRCIN1	1.27×10^{-3}	0.116
EPS8	1.27×10^{-3}	0.345
LRCH4	1.31×10^{-3}	0.037
SQRDL	1.32×10^{-3}	0.162
CDK5R1	1.35×10^{-3}	0.030
MICB	1.35×10^{-3}	0.049
HMGCL	1.37×10^{-3}	0.061
HIVEP2	1.37×10^{-3}	0.040
ZNF783	1.40×10^{-3}	0.137
NFKBIZ	1.40×10^{-3}	0.224
ITGA4	1.41×10^{-3}	0.205
NRARP	1.42×10^{-3}	0.143
TGFB1I1	1.42×10^{-3}	0.098
CPM	1.43×10^{-3}	0.222
FAM43A	1.43×10^{-3}	0.129
SORL1	1.43×10^{-3}	0.122
HDAC7	1.44×10^{-3}	0.138
TMEM134	1.46×10^{-3}	0.076

Table S2. Significantly differentially methylated genes in benign/low-grade and high-grade cartilage tumors. (*continued*)

Strongly Methylated in High-Grade Tumors (*n* = 592)		
Gene	***p*-Value**	**Difference in β-Value**
ARHGDIB	1.46×10^{-3}	0.108
RGS9BP	1.46×10^{-3}	0.050
DKFZp686O24166	1.48×10^{-3}	0.290
LARP1	1.51×10^{-3}	0.115
MAP4K2	1.52×10^{-3}	0.053
SPRY1	1.54×10^{-3}	0.181
SBK1	1.55×10^{-3}	0.234
ABLIM1	1.56×10^{-3}	0.194
RALGAPA2	1.57×10^{-3}	0.059
BANP	1.58×10^{-3}	0.024
DKFZp761E198	1.58×10^{-3}	0.047
SLC38A2	1.60×10^{-3}	0.048
ESRP2	1.62×10^{-3}	0.109
ANP32A	1.65×10^{-3}	0.061
ITPR3	1.65×10^{-3}	0.055
SLFN12L	1.66×10^{-3}	0.300
TMPRSS8	1.67×10^{-3}	0.221
DGKE	1.69×10^{-3}	0.099
ARPC1B	1.72×10^{-3}	0.181
CORIN	1.72×10^{-3}	0.112
SLC38A10	1.74×10^{-3}	0.095
MYO15A	1.74×10^{-3}	0.171
MTMR9L	1.76×10^{-3}	0.116
LRMP	1.77×10^{-3}	0.098
SIGIRR	1.78×10^{-3}	0.114
BEST4	1.78×10^{-3}	0.218
PVT1	1.79×10^{-3}	0.026
NRTN	1.79×10^{-3}	0.251
PLEKHG3	1.80×10^{-3}	0.216
NFIC	1.82×10^{-3}	0.121
KCNMB4	1.86×10^{-3}	0.106
TTC23L	1.87×10^{-3}	0.130
LSP1	1.88×10^{-3}	0.128
PNPLA7	1.90×10^{-3}	0.070
LYSMD2	1.90×10^{-3}	0.118
CES8	1.91×10^{-3}	0.156
PARP10	1.93×10^{-3}	0.042

Table S2. Significantly differentially methylated genes in benign/low-grade and high-grade cartilage tumors. (*continued*)

Strongly Methylated in High-Grade Tumors (*n* = 592)		
Gene	***p*-Value**	**Difference in β-Value**
GALK2	1.94×10^{-3}	0.038
LRRC14	1.95×10^{-3}	0.091
RASSF5	1.95×10^{-3}	0.068
VILL	1.95×10^{-3}	0.211
CYB5A	1.96×10^{-3}	0.308
SLMO2	1.97×10^{-3}	0.045
NEDD9	1.99×10^{-3}	0.036
MIR142	1.99×10^{-3}	0.121
LOC100268168	1.99×10^{-3}	0.070
RPL26L1	1.99×10^{-3}	0.070
FOXN3	1.99×10^{-3}	0.082
IL12RB2	2.00×10^{-3}	0.266
FXYD5	2.02×10^{-3}	0.109
FHIT	2.05×10^{-3}	0.107
TNK1	2.05×10^{-3}	0.099
ZNF710	2.05×10^{-3}	0.035
NT5DC3	2.05×10^{-3}	0.169
HPDL	2.06×10^{-3}	0.209
UBE2E2	2.08×10^{-3}	0.180
USP45	2.08×10^{-3}	0.005
SLC25A30	2.09×10^{-3}	0.028
C16orf86	2.10×10^{-3}	0.142
C16orf48	2.10×10^{-3}	0.142
ZBTB12	2.11×10^{-3}	0.036
STX12	2.11×10^{-3}	0.031
GFI1	2.12×10^{-3}	0.141
TMC6	2.13×10^{-3}	0.095
CD300A	2.14×10^{-3}	0.163
FLJ36777	2.14×10^{-3}	0.240
DLG4	2.14×10^{-3}	0.096
ZNF321	2.14×10^{-3}	0.017
S100A6	2.15×10^{-3}	0.201
SIAH2	2.15×10^{-3}	0.034
TTC17	2.20×10^{-3}	0.021
RASGRP1	2.20×10^{-3}	0.074
PCNX	2.20×10^{-3}	0.010
ABCA1	2.22×10^{-3}	0.187

Table S2. Significantly differentially methylated genes in benign/low-grade and high-grade cartilage tumors. (*continued*)

Strongly Methylated in High-Grade Tumors (*n* = 592)		
Gene	***p*-Value**	**Difference in β-Value**
IVNS1ABP	2.22×10^{-3}	0.066
C5orf24	2.24×10^{-3}	0.025
DNM1	2.24×10^{-3}	0.060
UHRF1	2.25×10^{-3}	0.072
PTPN7	2.26×10^{-3}	0.087
B3GALT4	2.28×10^{-3}	0.128
TAF8	2.28×10^{-3}	0.014
LATS1	2.30×10^{-3}	0.008
NINJ2	2.30×10^{-3}	0.094
LASP1	2.30×10^{-3}	0.025
C2CD2L	2.31×10^{-3}	0.032
NAPRT1	2.31×10^{-3}	0.245
ZNF763	2.31×10^{-3}	0.259
EVL	2.35×10^{-3}	0.051
PER2	2.39×10^{-3}	0.083
VIPR1	2.40×10^{-3}	0.218
TSPYL5	2.40×10^{-3}	0.174
HUS1	2.42×10^{-3}	0.126
RAC2	2.42×10^{-3}	0.146
RPS6KL1	2.43×10^{-3}	0.161
CELSR3	2.44×10^{-3}	0.162
COMMD10	2.45×10^{-3}	0.017
LRRC34	2.59×10^{-3}	0.241
AIG1	2.60×10^{-3}	0.006
AES	2.62×10^{-3}	0.204
CORO1B	2.63×10^{-3}	0.018
UBA2	2.64×10^{-3}	0.029
RRN3P1	2.65×10^{-3}	0.251
PDE6B	2.69×10^{-3}	0.061
C14orf182	2.69×10^{-3}	0.211
PLAU	2.70×10^{-3}	0.198
C10orf55	2.70×10^{-3}	0.198
APBB1IP	2.71×10^{-3}	0.225
WHSC1L1	2.72×10^{-3}	0.303
H2AFY	2.72×10^{-3}	0.059
AKAP1	2.72×10^{-3}	0.032
SLC38A1	2.75×10^{-3}	0.252

Table S2. Significantly differentially methylated genes in benign/low-grade and high-grade cartilage tumors. (*continued*)

Strongly Methylated in High-Grade Tumors (*n* = 592)		
Gene	***p*-Value**	**Difference in β-Value**
ATP1A3	2.75×10^{-3}	0.125
NR1I2	2.77×10^{-3}	0.196
COL23A1	2.82×10^{-3}	0.070
PCGF5	2.82×10^{-3}	0.083
C9orf142	2.86×10^{-3}	0.101
KIAA1324	2.86×10^{-3}	0.075
C1orf194	2.86×10^{-3}	0.075
CNDP2	2.89×10^{-3}	0.030
IRF4	2.94×10^{-3}	0.082
PRR5	2.96×10^{-3}	0.056
PRR5-ARHGAP8	2.96×10^{-3}	0.056
TXNRD2	2.97×10^{-3}	0.108
NIPAL1	2.99×10^{-3}	0.032
TBL1XR1	2.99×10^{-3}	0.023
TMC8	3.01×10^{-3}	0.093
C1orf59	3.04×10^{-3}	0.183
ZNF620	3.04×10^{-3}	0.045
FIP1L1	3.09×10^{-3}	0.030
DPP4	3.11×10^{-3}	0.143
DAPP1	3.15×10^{-3}	0.092
ZDHHC23	3.15×10^{-3}	0.041
ZBTB22	3.19×10^{-3}	0.042
UCP2	3.20×10^{-3}	0.223
PRDM8	3.21×10^{-3}	0.078
EZR	3.21×10^{-3}	0.087
RHOF	3.22×10^{-3}	0.083
ATP6V0C	3.22×10^{-3}	0.085
GPR137B	3.23×10^{-3}	0.051
CSRP1	3.28×10^{-3}	0.043
SPRED1	3.30×10^{-3}	0.129
BCL3	3.31×10^{-3}	0.046
C5orf56	3.37×10^{-3}	0.041
HIST1H3G	3.40×10^{-3}	0.244
GRIN2D	3.42×10^{-3}	0.130
CLIC5	3.44×10^{-3}	0.066
CTSC	3.45×10^{-3}	0.114
HLA-F	3.46×10^{-3}	0.110

Difference in β-value: high-grade β-value minus benign/low-grade β-value.

Table S3. Detailed list of all compounds included in the epigenetics compound library (L1900, Selleckchem).

Compound Class	Number	Product Name	Specific Targets
Aurora Kinases	1	Alisertib	Aurora A
	2	Aurora A Inhibitor I	Aurora A
	3	MK-5108	Aurora A
	4	Danusertib	Aurora A, Abl, RET, TrkA, FGFR1, Aurora C, Aurora B
	5	MLN8054	Aurora A, Aurora B
	6	CCT129202	Aurora A, Aurora B, Aurora C
	7	ZM 447439	Aurora A, Aurora B, LCK, Src, MEK1
	8	CYC116	Aurora A, Aurora B, VEGFR2, FLT3, CDK2, CDK9, p70 S6K
	9	CCT137690	Aurora A, Aurora C, Aurora B
	10	PHA-680632	Aurora A, Aurora C, Aurora B, FGFR1, PLK1, FLT3, VEGFR3, VEGFR2, LCK
	11	Tozasertib	Aurora A, Aurora C, Aurora B, FLT3, Bcr-Abl
	12	Barasertib	Aurora B
	13	Hesperadin	Aurora B
	14	SNS-314 Mesylate	Aurora C, Aurora A, Aurora B
	15	AMG-900	Aurora C, Aurora B, Aurora A, p38α
Bromodomain and Extra-Terminal Motif Proteins	16	RVX-208	BD2
	17	I-BET-762	BRD2, BRD3, BRD4
	18	OTX015	BRD2, BRD3, BRD4
	19	PFI-1	BRD2, BRD4
	20	I-BET151	BRD3, BRD2, BRD4
	21	(+)-JQ1	BRD4
	22	CPI-203	BRD4, IL-6, MYC
	23	Bromosporine	CECR2, BRD9, BRD4, BRD2
Catechol-O-methyltransferases	24	Entacapone	Catechol-O-methyltransferase (COMT)
Cyclin-dependent Kinases	25	JNJ-7706621	CDK2, CDK1, Aurora A, Aurora B, CDK3, VEGFR2, CDK6, FGFR2, CDK4, GSK-3β, Tie-2, FGFR1, VEGFR3
DNA Methyltransferases	26	Azacitidine	DNA Methyltransferase
	27	Decitabine	DNA Methyltransferase
	28	RG108	DNA methyltransferase
	29	Zebularine	DNA Methyltransferase, Cytidine deaminase
	30	Procainamide HCl	DNA methyltransferase, Sodium channel
	31	SGI-1027	DNMT1, DNMT3B, DNMT3A
Epidermal Growth Factor Receptor	32	AG-490	EGFR
	33	CUDC-101	EGFR, HDAC1, HDAC6, HDAC3, HDAC5, HDAC2, HDAC4, HER2, HDAC10, HDAC9, HDAC8, HDAC7
	34	WHI-P154	EGFR, VEGFR, Src, JAK3

Table S3. Detailed list of all compounds included in the epigenetics compound library (L1900, Selleckchem). *(continued)*

Compound Class	Number	Product Name	Specific Targets
Fms Related Receptor Tyrosine Kinase 3	35	KW-2449	FLT3, Abl, FGFR1, Aurora A, JAK2, Kit, Src
	36	Pacritinib	FLT3, JAK2, TYK2, JAK3
	37	ENMD-2076	FLT3, RET, Aurora A, VEGFR3, Src, NTRK1, CSF-1R, LCK, FAK, PDGFRα, VEGFR2, BLK, FGFR2, YES1, Abl1, FGFR1, Fyn, JAK2, Kit, Aurora B
Histone Acetyltransferases	38	SGC-CBP30	CREBBP, EP300
	39	C646	p300/CBP
Histone Deacetylases	40	AR-42	HDAC
	41	Belinostat	HDAC
	42	Dacinostat	HDAC
	43	M344	HDAC
	44	Panobinostat	HDAC
	45	Scriptaid	HDAC
	46	Sodium Phenylbutyrate	HDAC
	47	Vorinostat	HDAC
	48	Givinostat	HDAC (Class I, IIA, IIB)
	49	Trichostatin A	HDAC (Class I, IIA, IIB)
	50	MC1568	HDAC (Class IIA)
	51	Valproic Acid	HDAC, Autophagy, GABA Receptor
	52	Romidepsin	HDAC1, HDAC2
	53	Quisinostat	HDAC1, HDAC2, HDAC11, HDAC10, HDAC4, HDAC5, HDAC8, HDAC3
	54	Mocetinostat	HDAC1, HDAC2, HDAC11, HDAC3
	55	Tacedinaline	HDAC1, HDAC2, HDAC3
	56	Entinostat	HDAC1, HDAC3
	57	CUDC-907	HDAC1, HDAC3, HDAC10, HDAC2, HDAC11, PI3Kα, HDAC6, PI3Kδ, PI3Kβ
	58	Resminostat	HDAC1, HDAC3, HDAC6
	59	Abexinostat	HDAC1, HDAC3, HDAC6, HDAC2, HDAC10, HDAC8
	60	Pracinostat	HDAC10, HDAC3, HDAC5, HDAC1, HDAC4, HDAC9, HDAC11, HDAC2, HDAC7, HDAC8
	61	RGFP966	HDAC3
	62	RG2833	HDAC3, HDAC1
	63	Nexturastat A	HDAC6
	64	Rocilinostat	HDAC6
	65	Tubacin	HDAC6
	66	Tubastatin A	HDAC6
	67	Tubastatin A HCl	HDAC6
	68	PCI-34051	HDAC8

Table S3. Detailed list of all compounds included in the epigenetics compound library (L1900, Selleckchem). *(continued)*

Compound Class	Number	Product Name	Specific Targets
Histone Deacetylases	69	Droxinostat	HDAC8, HDAC6, HDAC3
	70	TMP269	HDAC9, HDAC7, HDAC5, HDAC4
Histone Demethylases	71	OG-L002	KDM1A
	72	IOX1	KDM3A, KDM4C, KDM6B, KDM2A, KDM4E, KDM5C, PHD2
	73	GSK J4 HCl	KDM6B
Histone Methyltransferases	74	BIX 01294	KMT1C
	75	MM-102	KMT2A
	76	EPZ004777	KMT4
	77	EPZ5676	KMT4
	78	SGC 0946	KMT4
	79	EPZ-6438	KMT6
	80	3-Deazaneplanocin A	KMT6, S-adenosylhomocysteine hydrolase
Hypoxia-inducible Factors	81	IOX2	HIF-1α prolyl hydroxylase-2
	82	2-Methoxyestradiol	HIF-2α, Microtubules depolymerisation, HIF-1α
	83	FG-4592	HIF-α prolyl hydroxylase
Janus Kinases	84	CYT387	JAK1, JAK2, JAK3
	85	Filgotinib	JAK1, JAK2, TYK2, JAK3
	86	AZ 960	JAK2
	87	AZD1480	JAK2
	88	CEP-33779	JAK2
	89	LY2784544	JAK2, FLT3, JAK1, FLT4, FGFR2, TYK2, JAK3, TrkB, FGFR3, KDR, ALK, MUSK, Aurora A, MAP3K9
	90	TG101348	JAK2, FLT3, RET
	91	Ruxolitinib	JAK2, JAK1
	92	S-Ruxolitinib	JAK2, JAK1, TYK2
	93	Baricitinib	JAK2, JAK1, TYK2, JAK3
	94	XL019	JAK2, PDGFRβ, JAK1, FLT3, JAK3
	95	TG101209	JAK2, RET, FLT3, JAK3
	96	WP1066	JAK2, STAT3
	97	NVP-BSK805 2HCl	JAK2, TYK2, JAK3, JAK1
	98	TAK-901	JAK3, c-Src, CLK2, FGR, YES1, LRRK2, FLT3, Fyn, ARG, Axl, Hck, SNF1LK2, Abl, RET, TrkA, LCK, PTK5, Fms, FGFR2, EphB1, EphA1, ARK5, ITK, ALK2, CDK7, BLK, Aurora B, JAK2, EphB2, Aurora A, STK16, EphA2, BRK, EphB4, TNK2, FGFR1, EphA4, STK33, CLK1, AMPK, FES, SLK, Chk2, TYK2, BTK, FAK2, c-Kit, VEGFR2, FGFR3, ALK5, MAP3K9, CLK3, JAK1

Table S3. Detailed list of all compounds included in the epigenetics compound library (L1900, Selleckchem). *(continued)*

Compound Class	Number	Product Name	Specific Targets
Janus Kinases	99	AT9283	JAK3, JAK2, Aurora A, Aurora B, Abl1, GSK-3β, FGFR2, VEGFR3, Mer, RET, RSK2, RSK3, TYK2, YES, Abl, DRAK1, FGFR1, FGFR2, FGFR3, VEGFR1, FLT3, PDGFRα, PDK-1, PKCμ, RSK4, Src, VEGFR2
	100	Tofacitinib	JAK3, JAK2, JAK1
	101	Tofacitinib Citrate	JAK3, JAK2, JAK1
	102	ZM 39923 HCl	TGM2, JAK3, EGFR, JAK1
Lethal(3)Malignant Brain Tumor-Like Proteins	103	UNC669	L3MBTL1, L3MBTL3, L3MBTL4
	104	UNC1215	L3MBTL3
Monoamine Oxidases	105	Tranylcypromine HCl	MAO-B, MAO-A, LSD1
O6-Alkylguanine DNA Alkyltransferases	106	Lomeguatrib	MGMT
Poly(ADP-Ribose) Polymerases	107	3-Aminobenzamide	PARP
	108	AZD2461	PARP
	109	INO-1001	PARP
	110	PJ34	PARP
	111	PJ34 HCl	PARP
	112	Rucaparib	PARP
	113	AG-14361	PARP1
	114	Iniparib	PARP1
	115	BMN 673	PARP1, PARP2
	116	Olaparib	PARP2, PARP1
	117	UPF 1069	PARP2, PARP1
	118	Veliparib	PARP2, PARP1
	119	ME0328	PARP3, PARP1
Pim Kinases	120	SMI-4a	Pim1
	121	SGI-1776 free base	Pim1, FLT3, Pim3, Pim2
	122	AZD1208	Pim1, Pim3, Pim2
	123	CX-6258 HCl	Pim1, Pim3, Pim2
Sirtuins	124	Selisistat	SIRT1
	125	SRT1720	SIRT1
	126	Resveratrol	SIRT1, SIRT2, Quinonen reductase 2, IKK β, COX1, COX2, DNA polymerase α, LOX
	127	Quercetin	SIRT1, Src, PKC, PI3Kγ, PI3Kδ, PI3Kβ
	128	Sirtinol	SIRT2, SIRT1

The specific targets of the compounds are listed in order of increasing IC50 values determined in cell-free kinase activity assays (Selleckchem website).

Table S4. Detailed list of all the compounds included in the custom designed compound library for the HDAC inhibitor combination drug screen.

Compound Class	Product Name	Target	Solvent	Concentrations	Company
Apoptosis	YM155	Survivin	DMSO	0.1–1000 nM	Selleckchem
Bcl-2 Family Members	ABT-737	Bcl-2 / Bcl-xL / Bcl-w	DMSO	1–10,000 nM	Selleckchem
	AT101	Bcl-2 / Bcl-xL / Mcl-1	DMSO	1–10,000 nM	Selleckchem
	S63845	Mcl-1	DMSO	1–10,000 nM	Selleckchem
	Venetoclax	Bcl-2	DMSO	1–10,000 nM	Selleckchem
	WEHI-539	Bcl-xL	DMSO	1–10,000 nM	APExBIO
Cell Cycle Regulators	Rabusertib	CHK1	DMSO	1–10,000 nM	Selleckchem
	MK-5108	Aurora Kinase A	DMSO	1–10,000 nM	Selleckchem
	Volasertib	PLK1	DMSO	0.1–1000 nM	Selleckchem
Chemotherapy	Aclarubicin	Topoisomerase I & II	DMSO	0.1–1000 nM	APExBIO
	Cisplatin	DNA Replication	PBS	1–10,000 nM	LUMC Pharmacy
	Doxorubicin	Topoisomerase II	PBS	0.1–1000 nM	LUMC Pharmacy
	Temozolomide	DNA Replication	DMSO	0.01–100 µM	Selleckchem
DNA Damage Repair	Talazoparib	PARP	DMSO	1–10,000 nM	Selleckchem
Metabolism	CB-839	Glutaminase	DMSO	0.01–100 µM	Selleckchem
	Chloroquine Diphosphate	Autophagy / Glutamate Dehydrogenase	PBS	1–100 µM	Selleckchem
	FK866	NAMPT	DMSO	0.008–80 nM	Sigma-Aldrich
	Metformin HCl	AMPK / Glutaminase	RPMI	0.1–10 mM	Selleckchem
	Sapanisertib	mTOR	DMSO	0.01–100 nM	Selleckchem
Protein Degradation	Bortezomib	20S Proteasome	DMSO	0.1–1000 nM	Selleckchem

Supplementary figures

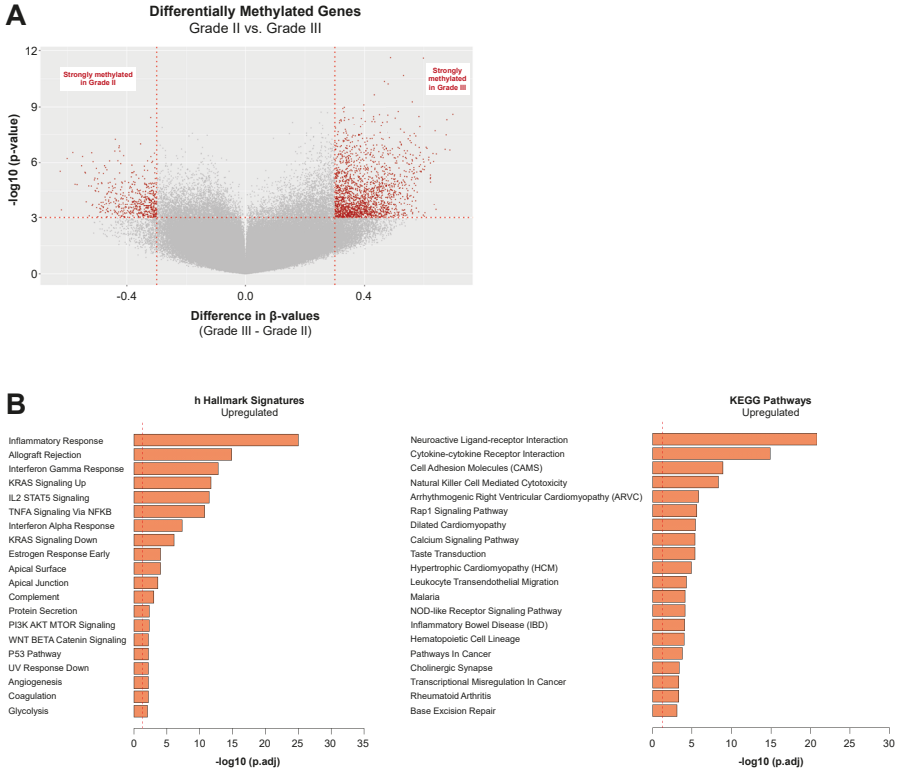

Figure S1. Hypermethylation keeps increasing even within high-grade *IDH* mutant chondrosarcomas and mainly affects signal transduction and inflammation related genes.
(A) Volcano plot of differentially methylated genes between chondrosarcoma grade II and grade III tumors. Vertical red lines indicate a difference in β-values of at least 0.3 between the two groups. Significantly differentially methylated genes are indicated with red (cut-off at $p < 0.001$). **(B)** EGSEA analysis performed on the significantly differentially methylated gene sets. Both h Hallmark signatures and KEGG pathways identified that mainly genes related to signal transduction and inflammation were affected.

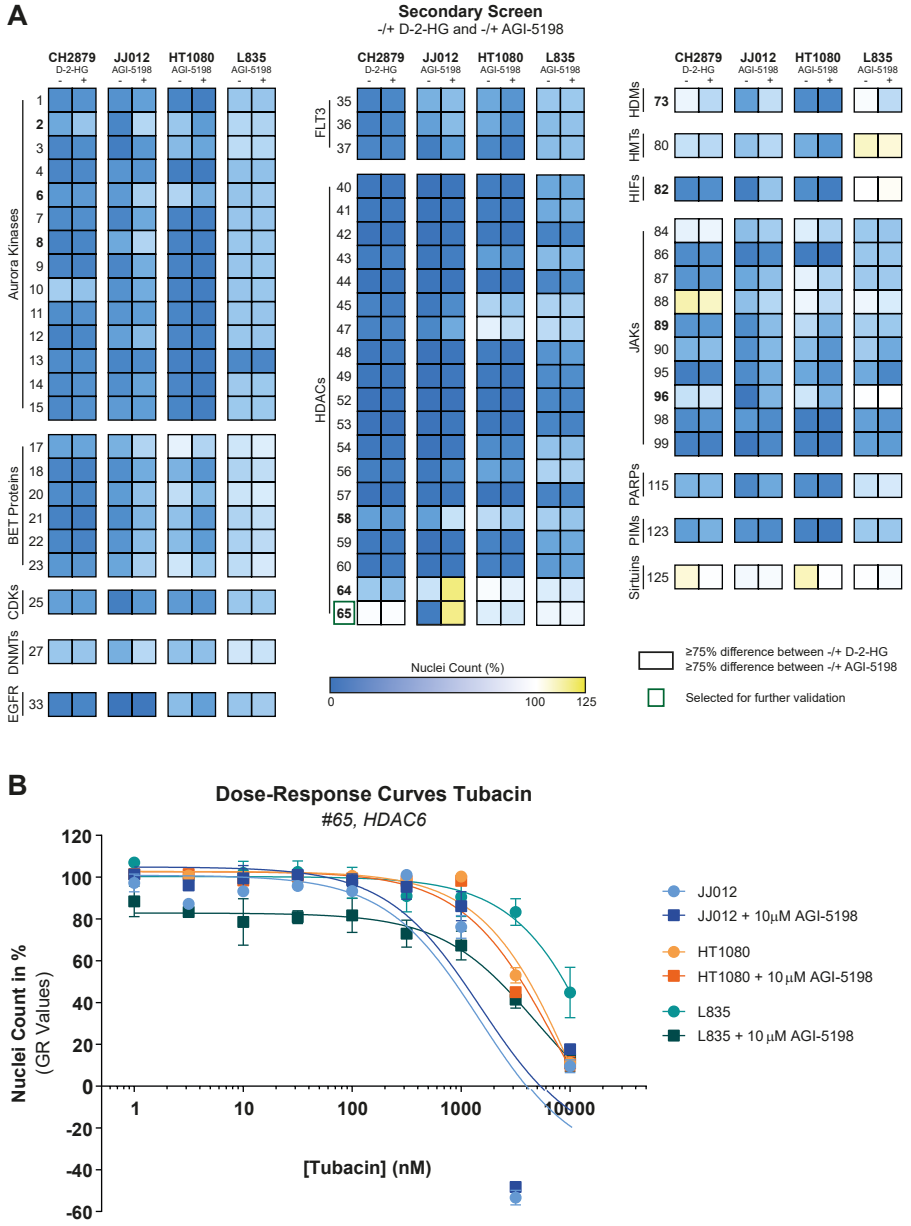

Figure S2. Drug screening does not identify a synthetic lethal interaction between epigenetic regulators and *IDH* mutations.

(A) Heatmaps of the results from the secondary epigenetics compound screen, in which blue indicates growth inhibition and yellow growth induction. Five chondrosarcoma cell lines –/+ 10 μM AGI-5198 or –/+ 250 μM D-2-HG were treated with 61 compounds at a concentration of 2 μM for 72 h. One potential synthetic lethal interaction (≥75% difference between with or without AGI-5198 treatment) was observed in the JJ012 cell line. **(B)** Dose-response curves of compound #65 (tubacin), a specific HDAC6 inhibitor for three *IDH1* mutant chondrosarcoma cell lines. Short-term treatment with 10 μM AGI-5198 (i.e., 72 h pre-exposure) did not rescue the effect of tubacin in all three cell lines. Dose-response curves were corrected for growth rate (GR values). Data points represent the mean of one experiment performed in triplicate ± standard deviation.

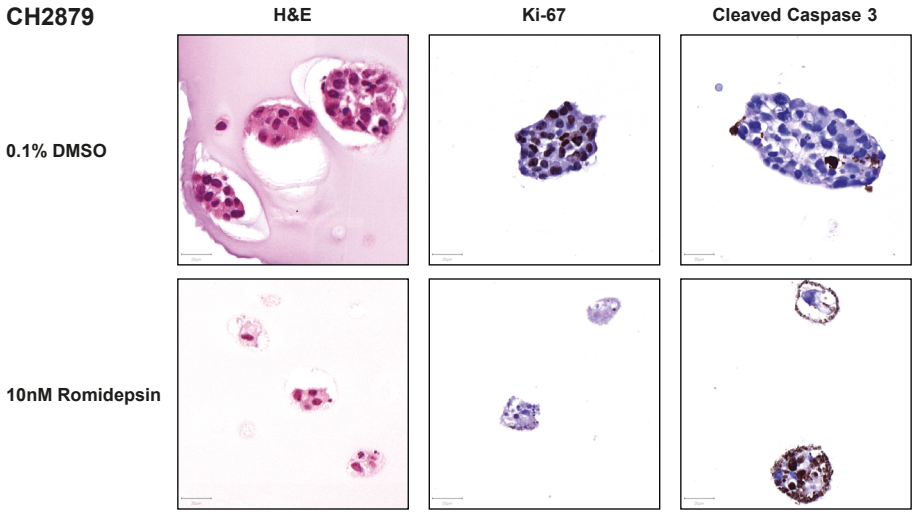

Figure S3. Romidepsin inhibits cell proliferation and induces apoptosis in 3D cell cultures of chondrosarcoma cell lines.

Haematoxylin and Eosin (H&E), Ki-67, and cleaved caspase 3 stains performed on CH2879 spheroids after 72 h of treatment with 0.1% DMSO or 10 nM romidepsin. As compared to the control, romidepsin inhibits proliferation (reduced Ki-67 levels and smaller spheroids) and induces apoptosis (increased cleaved caspase 3 levels) in CH2879 spheroids. Similar observations were made for JJ012 and SW1353 spheroids. Scale bar: 20 µm.

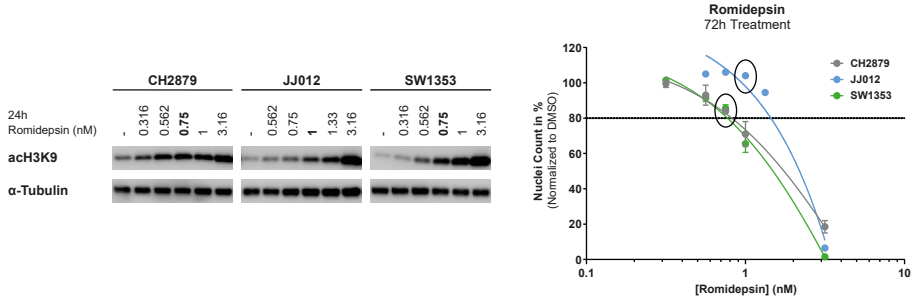

Figure S4. Low dose of romidepsin induces the level of histone 3 acetylation in chondrosarcoma cell lines, whilst cell viability is minimally affected.

Western blot for acH3K9 after 24 h treatment with low dosages of romidepsin (0.316 to 1.33 nM) and the corresponding cell viability after 72 h of treatment with these specific concentrations. Low romidepsin doses induced acH3K9 and showed a minimal effect on cell growth (>80% nuclei left). As a positive control, 24 h treatment with a high dose of romidepsin (3.16 nM) was used. α-Tubulin was used as a loading control. Whole blots with densitometry readings can be found in Figure S7E.

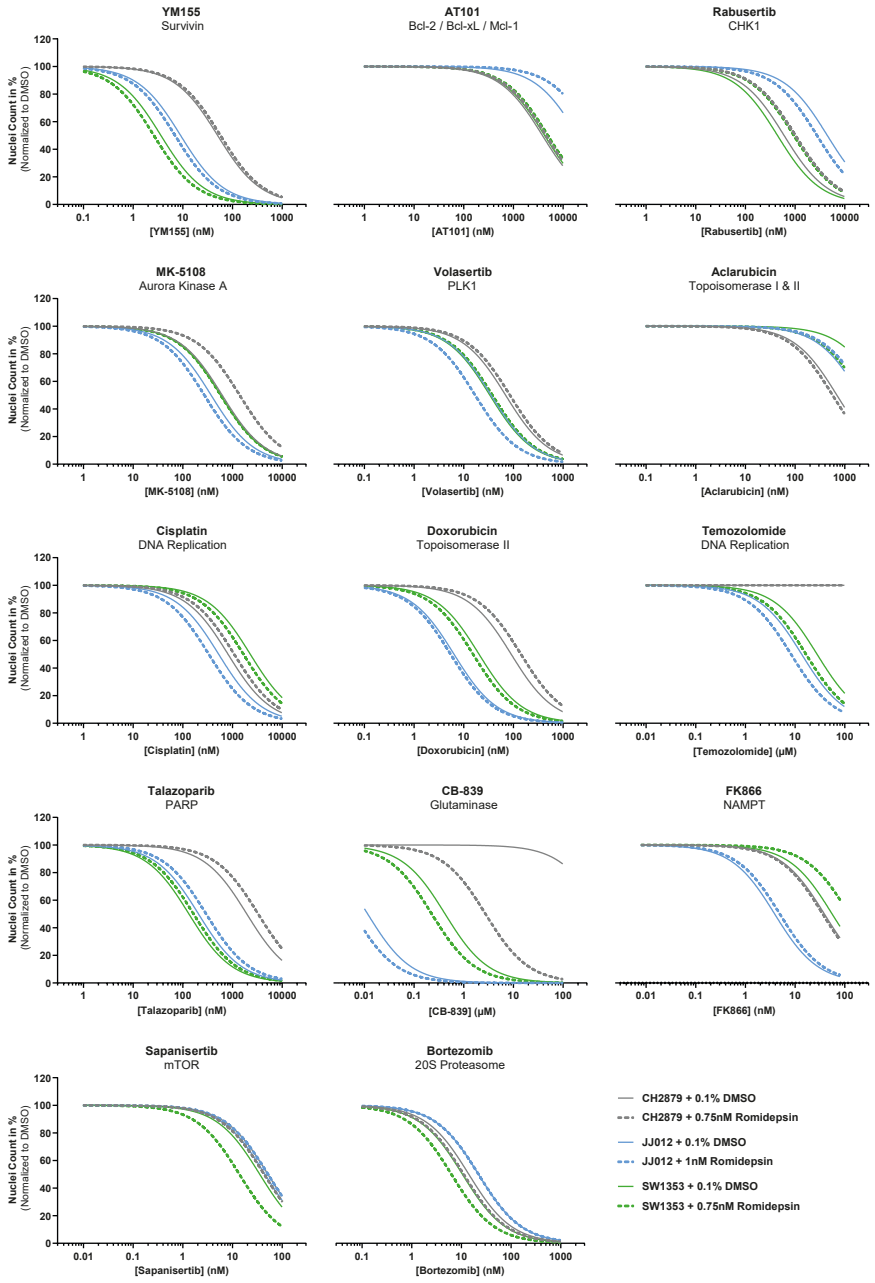

Figure S5. A selection of non-epigenetic drugs does not exhibit synergy in combination with a low dose of romidepsin.

Dose-response curves of the fourteen combination therapies that were not considered as a hit in in the HDAC inhibitor combination drug screen. Three chondrosarcoma cell lines were treated with twenty different non-epigenetic drugs in five concentrations (72 h) with or without romidepsin (96 h). A difference in nuclei count of ≥20% between –/+ romidepsin conditions was considered as a potential synergistic treatment combination. Graphs represent the normalized non-linear fit which was calculated based on the individual data points.

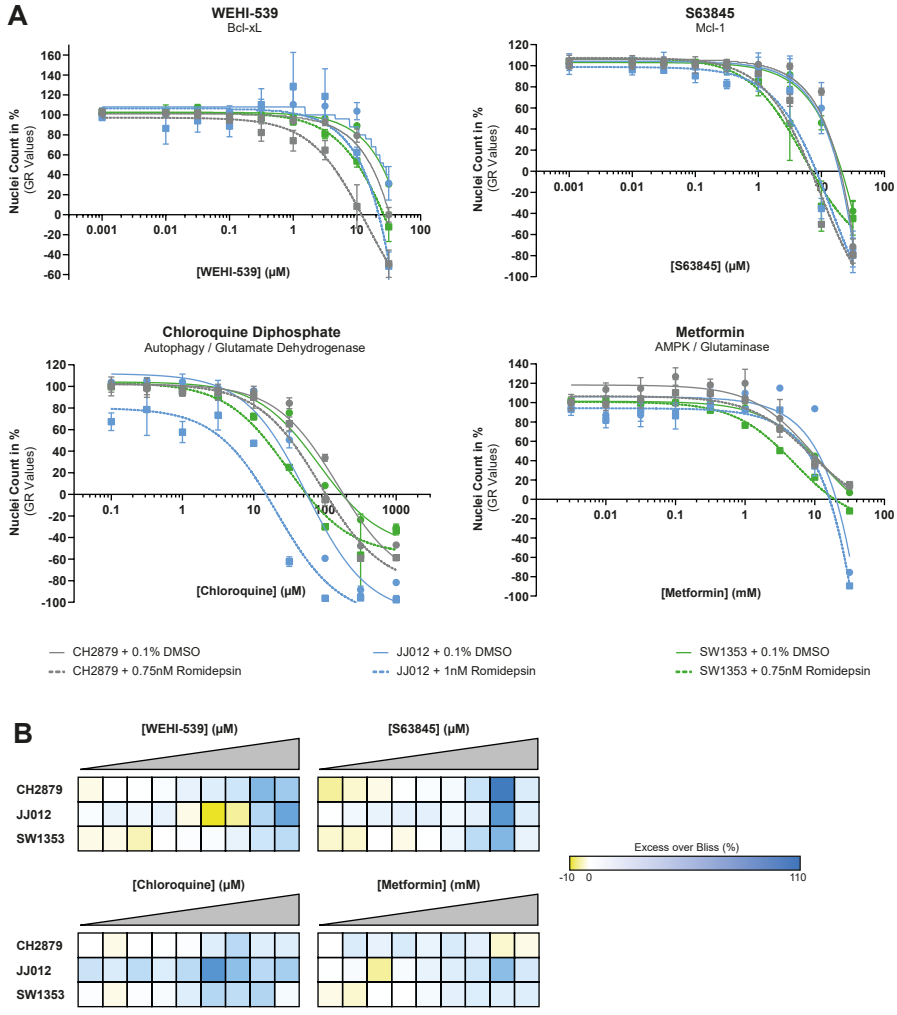

Figure S6. Romidepsin sensitizes chondrosarcoma cells to Bcl-2 family member inhibitors and metabolic compounds.

(A) Dose-response curves of single or combination treatment strategies after 72 h of treatment for three chondrosarcoma cell lines. Romidepsin treatment sensitized three chondrosarcoma cell lines to WEHI-539, S63845, chloroquine diphosphate, and metformin HCl. Data were corrected for growth rate (GR values). Data points represent the mean of one (i.e., chloroquine and metformin) or two (i.e., WEHI-539 and S63845) experiments performed in triplicate ± standard deviation. **(B)** Heatmaps of the calculated Excess over Bliss scores for the combination treatment strategies. Yellow represents antagonism, white represents additivity and blue represents synergy. All combination treatment strategies were synergistic, but synergy was less pronounced as compared to the combination treatments with ABT-737 and venetoclax.

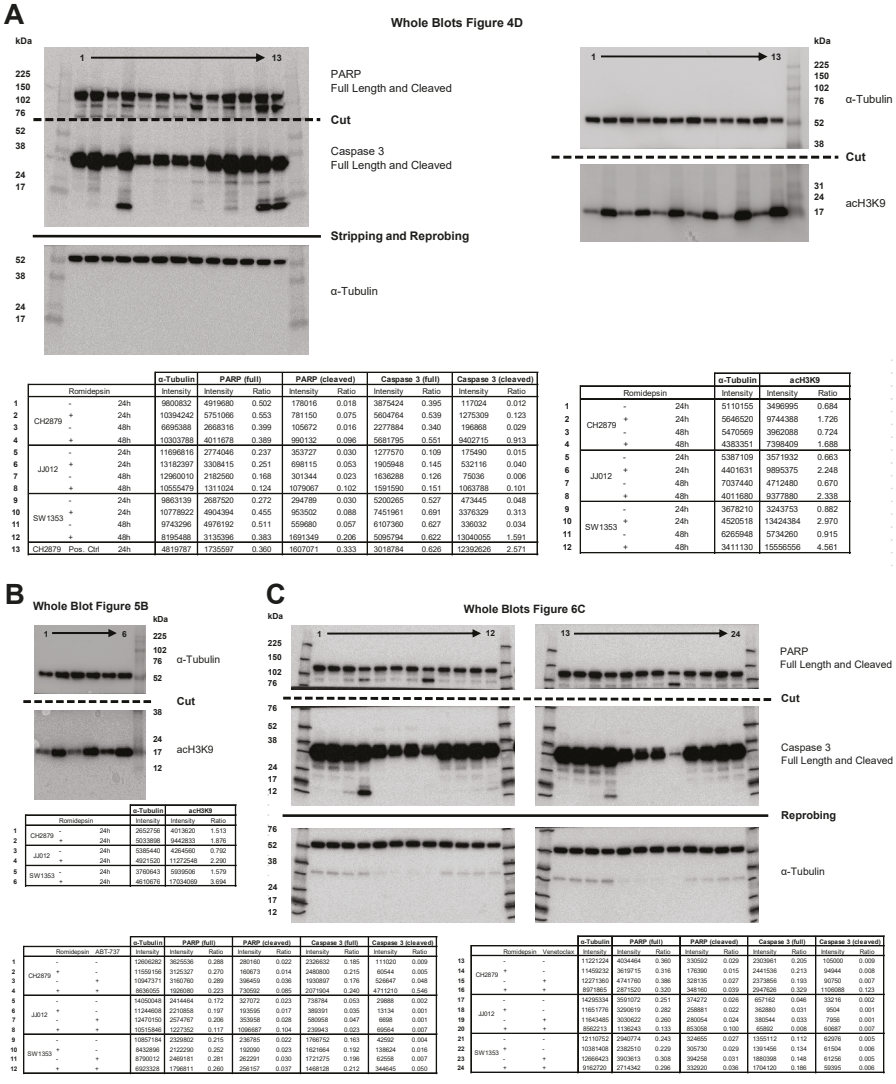

	Romidepsin		α-Tubulin Intensity	PARP (full) Intensity	PARP (full) Ratio	PARP (cleaved) Intensity	PARP (cleaved) Ratio	Caspase 3 (full) Intensity	Caspase 3 (full) Ratio	Caspase 3 (cleaved) Intensity	Caspase 3 (cleaved) Ratio
1	-	24h	9800832	4919680	0.502	178016	0.018	3875424	0.395	117024	0.012
2	CH2879 +	24h	10394242	5751066	0.553	781150	0.075	5604764	0.539	1275309	0.123
3	-	48h	6695388	2668316	0.399	105672	0.016	2277884	0.340	196868	0.029
4	+	48h	10303788	4011678	0.389	990132	0.096	5681795	0.551	9402715	0.913
5	-	24h	11698816	2774046	0.237	353727	0.030	1277570	0.109	175490	0.015
6	JJ012 +	24h	13182397	3308415	0.251	698115	0.053	1905948	0.145	532116	0.040
7	-	48h	12960010	2182560	0.168	301344	0.023	1636288	0.126	75036	0.006
8	+	48h	10555479	1311024	0.124	1079067	0.102	1591590	0.151	1063788	0.101
9	-	24h	9863139	2687520	0.272	294789	0.030	5200265	0.527	473445	0.048
10	SW1353 +	24h	10778922	4904394	0.455	953502	0.088	7451961	0.691	3376329	0.313
11	-	48h	9743296	4976192	0.511	559680	0.057	6107360	0.627	336032	0.034
12	+	48h	8195488	3135396	0.383	1691349	0.206	5095794	0.622	13040055	1.591
13	CH2879 Pos. Ctrl	24h	4819787	1735597	0.360	1607071	0.333	3018784	0.626	12392626	2.571

	Romidepsin		α-Tubulin Intensity	acH3K9 Intensity	acH3K9 Ratio
1	-	24h	5110155	3496995	0.684
2	CH2879 +	24h	5646520	9744388	1.726
3	-	48h	5470569	3962088	0.724
4	+	48h	4383351	7398409	1.688
5	-	24h	5387109	3571932	0.663
6	JJ012 +	24h	4401631	9895375	2.248
7	-	48h	7037440	4712480	0.670
8	+	48h	4011680	9377880	2.338
9	-	24h	3678210	3243753	0.882
10	SW1353 +	24h	4520518	13424384	2.970
11	-	48h	6265948	5734260	0.915
12	+	48h	3411130	15556556	4.561

	Romidepsin		α-Tubulin Intensity	acH3K9 Intensity	acH3K9 Ratio
1	-	24h	2652756	4013620	1.513
2	CH2879 +	24h	5033898	9442833	1.876
3	-	24h	5385440	4264560	0.792
4	JJ012 +	24h	4921520	11272548	2.290
5	-	24h	3760643	5939508	1.579
6	SW1353 +	24h	4610676	17034089	3.694

	Romidepsin	ABT-737	α-Tubulin Intensity	PARP (full) Intensity	PARP (full) Ratio	PARP (cleaved) Intensity	PARP (cleaved) Ratio	Caspase 3 (full) Intensity	Caspase 3 (full) Ratio	Caspase 3 (cleaved) Intensity	Caspase 3 (cleaved) Ratio
1	-	-	12606262	3625536	0.288	280160	0.022	2326632	0.185	111020	0.009
2	CH2879 +	-	11559156	3125327	0.270	160673	0.014	2480800	0.215	60544	0.005
3	-	+	10947371	3160760	0.289	396459	0.036	1930897	0.176	526847	0.048
4	+	+	8636055	1926080	0.223	730592	0.085	2071904	0.240	4711210	0.546
5	-	-	14050048	2414464	0.172	327072	0.023	736784	0.053	29888	0.002
6	JJ012 +	-	11244668	2210858	0.197	193595	0.017	380091	0.035	13134	0.001
7	-	+	12470150	2574767	0.206	353958	0.028	580958	0.047	6698	0.001
8	+	+	10515846	1227352	0.117	1096687	0.104	239943	0.023	69564	0.007
9	-	-	10857184	2329802	0.215	236785	0.022	1766752	0.163	42592	0.004
10	SW1353 +	-	8432896	2122290	0.252	192090	0.023	1621664	0.192	138624	0.016
11	-	+	8790012	2469181	0.281	262291	0.030	1721275	0.196	62558	0.007
12	+	+	6923328	1796811	0.260	256157	0.037	1468128	0.212	348645	0.050

	Romidepsin	Venetoclax	α-Tubulin Intensity	PARP (full) Intensity	PARP (full) Ratio	PARP (cleaved) Intensity	PARP (cleaved) Ratio	Caspase 3 (full) Intensity	Caspase 3 (full) Ratio	Caspase 3 (cleaved) Intensity	Caspase 3 (cleaved) Ratio
13	-	-	11221224	4034464	0.360	330592	0.029	2303961	0.205	105000	0.009
14	CH2879 +	-	11459232	3619715	0.316	176390	0.015	2441536	0.213	94944	0.008
15	-	+	12271360	4741760	0.386	328135	0.027	2373856	0.193	90750	0.007
16	+	+	8971865	2871520	0.320	348160	0.039	2947626	0.329	1106088	0.123
17	-	-	14295334	3591072	0.251	374272	0.026	657162	0.046	33216	0.002
18	JJ012 +	-	11651776	3290819	0.282	258881	0.022	362880	0.031	9504	0.001
19	-	+	11643485	3030622	0.260	280054	0.024	380544	0.033	7956	0.001
20	+	+	8562213	1136243	0.133	853058	0.100	65892	0.008	60867	0.007
21	-	-	12110752	2940774	0.243	324655	0.027	1355112	0.112	62976	0.005
22	SW1353 +	-	10381408	2382510	0.229	305730	0.029	1391456	0.134	61504	0.006
23	-	+	12666423	3903613	0.308	394258	0.031	1860398	0.148	61256	0.005
24	+	+	8162726	2714342	0.256	332920	0.036	1704120	0.186	59595	0.006

Figure S7. Whole blots with densitometry readings from the performed western blots.
Whole blots with densitometry readings from the western blots depicted in **(A)** Figure 4D, **(B)** Figure 5B, **(C)** Figure 6C, **(D)** Figure 6D, and **(E)** Figure S4.

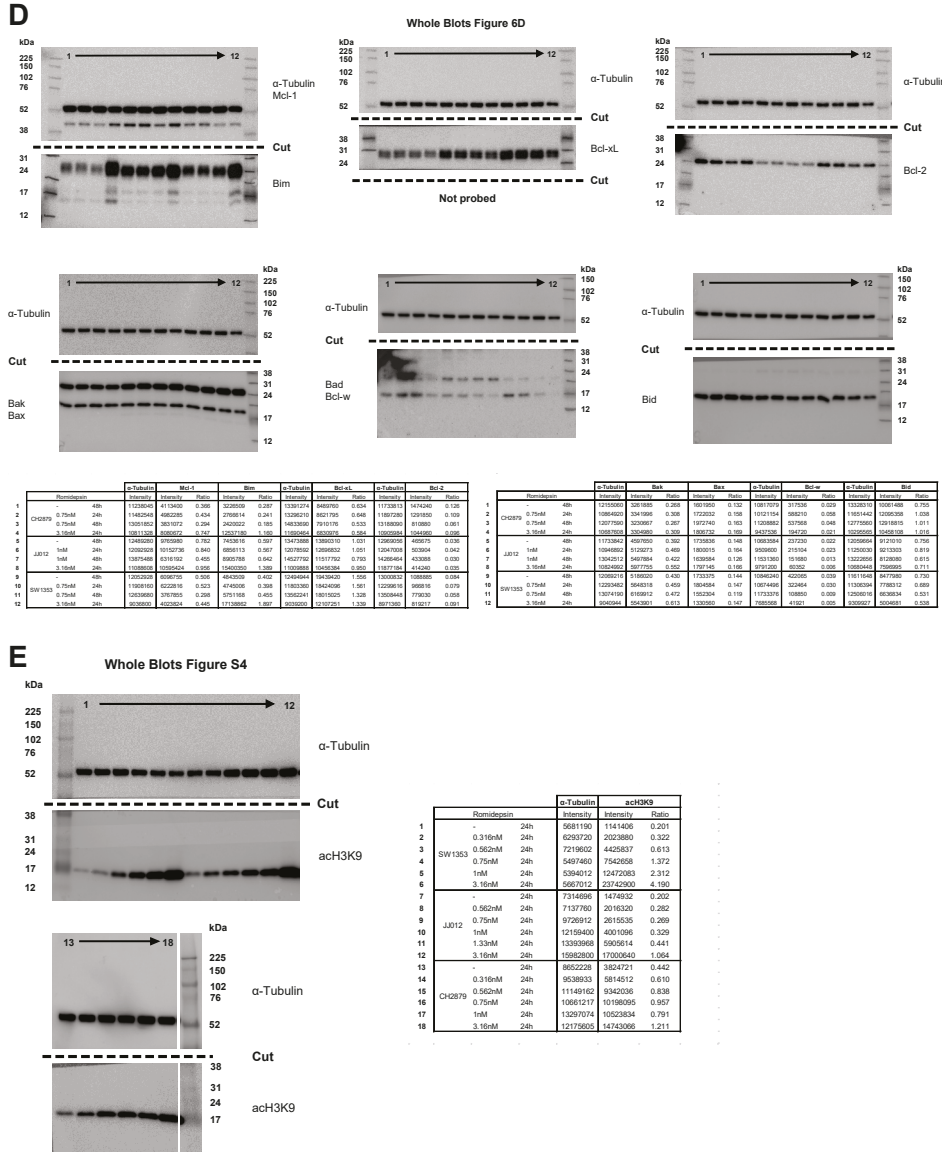

			α-Tubulin	Mcl-1		Bim		α-Tubulin	Bcl-xL		α-Tubulin	Bcl-2	
	Romidepsin		Intensity	Intensity	Ratio	Intensity	Ratio	Intensity	Intensity	Ratio	Intensity	Intensity	Ratio
1	-	48h	11238045	4113400	0.366	3226509	0.287	13391274	8469760	0.634	11733813	1474240	0.126
2	CH2879	0.75nM	24h	11482548	4982285	0.434	2766614	0.241	13298210	8531795	0.648	11897280	1291850	0.109
3		0.75nM	48h	13051852	3831072	0.294	2420022	0.185	14833690	7910176	0.533	13188390	810880	0.061
4		3.16nM	24h	10811328	8086672	0.747	12537180	1.159	11690464	6830976	0.584	10909984	1044960	0.096
5	JJ012	-	48h	12489283	9765980	0.782	7453616	0.597	13473888	13890310	1.031	12569056	469575	0.036
6		1nM	24h	12092928	10152736	0.840	6856113	0.567	12858832	13598832	1.057	12047008	503904	0.042
7		1nM	48h	13875488	6316192	0.455	8905788	0.642	14527792	11517792	0.793	14266464	453088	0.030
8		3.16nM	24h	11088608	10595424	0.956	15402050	1.389	11600864	10456394	0.902	11877184	414240	0.035
9		-	48h	12002928	6596795	0.566	4843509	0.402	12494944	19436420	1.556	13000832	1088885	0.084
10	SW1353	0.75nM	24h	11908160	6222816	0.523	4745006	0.398	11803360	18424096	1.561	12229616	966816	0.079
11		0.75nM	48h	12639680	3767855	0.298	4751168	0.455	13562241	18015025	1.328	13508448	779030	0.058
12		3.16nM	24h	9036800	4023824	0.445	17138862	1.897	9039200	12107251	1.339	8973389	819217	0.091

			α-Tubulin	Bak		Bax		α-Tubulin	Bcl-w		α-Tubulin	Bid	
	Romidepsin		Intensity	Intensity	Ratio	Intensity	Ratio	Intensity	Intensity	Ratio	Intensity	Intensity	Ratio
1	-	48h	12155080	3261885	0.268	1601950	0.132	10817079	317536	0.029	13328310	10081488	0.756
2	CH2879	0.75nM	24h	10864020	3341996	0.308	1722032	0.158	10121154	568210	0.056	11651442	12095358	1.038
3		0.75nM	48h	13077580	3230987	0.247	1972740	0.163	12008882	537988	0.046	13775560	12918815	1.011
4		3.16nM	24h	10987828	3304980	0.309	1806732	0.169	9437536	194720	0.021	10295568	10458108	1.016
5	JJ012	-	48h	11733842	4597650	0.392	1733838	0.148	10663584	237230	0.022	12056644	9120110	0.756
6		1nM	24h	10944882	5129273	0.469	1803015	0.164	9909600	215104	0.023	11250030	9213303	0.819
7		1nM	48h	13042512	5467884	0.422	1639584	0.126	11531369	151680	0.013	13222656	8128080	0.615
8		3.16nM	24h	10824662	5877755	0.552	1797145	0.166	9797200	80352	0.008	10880448	7566995	0.711
9		-	48h	12069216	5186920	0.430	1733375	0.144	10846240	422065	0.039	11611648	8477980	0.730
10	SW1353	0.75nM	24h	12293462	5648318	0.459	1804584	0.147	10874496	322464	0.030	11308394	7788312	0.689
11		0.75nM	48h	13074190	6169912	0.472	1952304	0.119	11733376	108850	0.009	12508016	6638634	0.531
12		3.16nM	24h	9046944	5543901	0.613	1330560	0.147	7885568	41921	0.005	8399927	5004681	0.539

			α-Tubulin	acH3K9	
	Romidepsin		Intensity	Intensity	Ratio
1	-	24h	5681190	1141406	0.201
2	SW1353	0.316nM	24h	6293720	2023880	0.322
3		0.562nM	24h	7219602	4425837	0.613
4		0.75nM	24h	5497460	7542658	1.372
5		1nM	24h	5394012	12472083	2.312
6		3.16nM	24h	5667012	23742900	4.190
7	JJ012	-	24h	7314696	1474932	0.202
8		0.562nM	24h	7137760	2016320	0.282
9		0.75nM	24h	9726912	2615535	0.269
10		1nM	24h	12159400	4001096	0.329
11		1.33nM	24h	13393968	5905614	0.441
12		3.16nM	24h	15982800	17000640	1.064
13	CH2879	-	24h	8652228	3824721	0.442
14		0.316nM	24h	9538933	5814512	0.610
15		0.562nM	24h	11149162	9342036	0.838
16		0.75nM	24h	10661217	10198095	0.957
17		1nM	24h	13297074	10523834	0.791
18		3.16nM	24h	12175605	14743086	1.211

Figure S7. Whole blots with densitometry readings from the performed western blots. *(continued)*
Whole blots with densitometry readings from the western blots depicted in **(A)** Figure 4D, **(B)** Figure 5B, **(C)** Figure 6C, **(D)** Figure 6D, and **(E)** Figure S4.